



Universidad
de La Laguna



Grado en Física

Trabajo Fin de Grado

USING GLOBULAR CLUSTERS AND
SYNTHETIC SIMPLE STELLAR POPULATIONS
TO TEST STELLAR EVOLUTION MODELS
AND THE PERFORMANCE OF STAR
FORMATION HISTORY DERIVATION
ALGORITHMS FOR GAIA DATA.

Autor:

DAVID MIRABAL BETANCORT

Tutoras:

CARME GALLART GALLART

EMMA FERNÁNDEZ ALVAR

July 2023

Contents

1. Abstract	3
2. Introduction	5
3. Goals	7
4. The Data	8
4.1. Observational data	8
4.1.1. Source catalogue with photometric, astrometric and membership probabilities. Clusters selection	8
4.1.2. Distances to clusters	10
4.1.3. Metallicities of globular clusters	12
4.1.4. Extinction	13
4.2. Synthetic data	14
4.2.1. Synthetic clusters at old ages	14
4.2.2. Synthetic clusters at all ages	16
5. Methodology	17
5.1. Transformation to the absolute magnitude plane	17
5.2. Cluster members selection	17
5.3. Comparison with isochrones	20
5.3.1. Comparing between models: BaSTI and PARSEC	20
5.3.2. Individual BaSTI and PARSEC fits	21
5.4. The SFH calculation method	21
5.4.1. Testing the bin size of the SFH calculation method	22
6. Results	24
6.1. The accuracy of extinction and metallicities from the literature	24
6.2. Differences between the BaSTI and PARSEC stellar evolution libraries	25
6.3. Individual BaSTI and PARSEC fits	25
6.4. Is it possible to determine ages and metallicities of GCs with this method?	27
6.5. Testing the SFH calculation method with synthetic clusters	28
6.5.1. Accuracy and precision of the SFH calculation as a function of bin size	29
6.5.2. Testing the SFH calculation method for synthetic GCs	34
7. Conclusions and future work	36
7.1. Observational data quality	36

7.2. On the comparison between GC CMDs and isochrones. Differences between BaSTI and PARSEC	36
7.3. Performance of the SFH calculation method	37
8. Acknowledge	39
9. Code availability	39
References	39
A. Appendix: Real globular clusters	41
A.1. Distances to clusters	41
A.2. Cluster Members selection	42
A.3. Comparing between models: BaSTI and PARSEC	44
A.4. Individually BaSTI fits	46
B. Appendix: Synthetic data	48
B.1. Synthetic data selection at old ages	48
B.2. Gaussian fitting for the SFH calculation of the 15000 stars sample	50
B.3. Gaussian fitting for the SFH calculation of the 100000 stars sample	51
B.4. SFH of all recast	52
B.5. Accuracy in age of each age bin size for bursts calculated	54

1. Abstract

This study focuses on comparing observed color-magnitude diagrams of globular clusters with theoretical models. The results show differences between theoretical models and the need to improve the accuracy of the literature data so that the models match to the clusters diagrams. Also, the research project hosting this TFG has developed a method called CMDft.Gaia, which calculates the star formation history by comparing observed color-magnitude diagrams with simulated ones. This work examines the accuracy and precision of CMDft.Gaia using synthetic clusters.

Los cúmulos estelares (CEs) son conjuntos de estrellas con composición química (metalicidad) y edad similar que ofrecen oportunidades de gran valor para comprender la evolución estelar. En las escalas de tiempo humanas no es posible analizar la evolución de una estrella en sus propias escalas de tiempo, por lo que se necesitan estas poblaciones para entender la física de las estrellas. Los cúmulos globulares (CG) son CEs con edades viejas y situados normalmente en el halo de la Vía Láctea, mientras que los cúmulos abiertos suelen ser CEs con edades jóvenes y menos densos que los CGs. Ambos nos proporcionan la capacidad de comprobar y mejorar los modelos teóricos sobre evolución estelar en un rango de edades viejas. Este va a ser uno de los objetivos de este trabajo.

Por otro lado, el proyecto de investigación en el que está incluido este TFG ha desarrollado un método complejo (CMDft.Gaia, [Ruiz-Lara et al., 2022](#)) para calcular la historia de formación estelar (HFE) (Gallart et al. in prep) a partir de comparar diagramas color-magnitud (DCM) observados con DCM simulados a partir de modelos teóricos de evolución estelar. CMDft.Gaia calcula la combinación de poblaciones estelares sintéticas simples (que contienen rangos muy pequeños de edad y metalicidad, al igual que los cúmulos observados) que mejor reproduce el DCM observado (input data). Para crear estas poblaciones es necesario un DCM teórico (diagrama madre) en el que se conozcan las edades y metalicidades de sus estrellas. Al rango de edad de estas poblaciones simples lo llamaremos *bin* de edad. En este trabajo se comprueban algunos aspectos del correcto funcionamiento de CMDft.Gaia, además de su precisión y exactitud, usando datos simulados.

Para el primer objetivo de este trabajo, la comprobación de los modelos de evolución estelar a edades viejas y en un rango de metalicidad, se seleccionan 10 CGs y, con datos del satélite *Gaia*, se comparan sus DCM con isocronas teóricas creadas con modelos de dos librerías de evolución estelar.

Para poder comparar el DCM de los cúmulos con isocronas, es necesario transformarlo primero al plano de magnitudes absolutas. Para ello, en primer lugar es necesario conocer la distancia. Se usa para cada estrella del mismo cúmulo la distancia calculada por [Baumgardt & Vasiliev \(2021\)](#). Esto es porque las distancias medidas a partir de la paralaje de *Gaia* no son lo suficientemente precisas para el objetivo de este trabajo: al estar estos cúmulos en el halo de la Vía Láctea, se encuentran a grandes distancias por lo que las medidas de la paralaje tienen mucho error. En segundo lugar, es necesario corregir de la extinción interestelar para lo que se usan los valores proporcionados en el catálogo de [Harris \(1996\)](#). Finalmente, para minimizar la influencia de los errores fotométricos se descartan las estrellas localizadas en los centros de los cúmulos y afectadas por *crowding*. Tras esto se seleccionan las estrellas más probables de pertenecer al cúmulo con las probabilidades calculadas por [Vasiliev & Baumgardt \(2021\)](#) usando, entre otros, la posición en el cielo, los movimientos propios, la paralaje y la distancia angular al centro del cúmulo.

Después del tratamiento de los datos, los CGs se comparan con isocronas de dos librerías de modelos de evolución estelar, BaSTI y PARSEC. En un DCM, se muestran las estrellas de cada cúmulo junto a isocronas teóricas de edades viejas y composiciones químicas encontradas en la literatura. Se encuentran diferencias entre los modelos, siendo las isocronas de PARSEC más rojas que las de BaSTI. Asimismo, se comprueba que, en la mayoría de los casos, usando la extinción y la metalicidad obtenida de la literatura no se consigue un buen acuerdo entre el DCM y las isocronas.

Por esta razón, se cambia individualmente la extinción de cada cúmulo y la metalicidad de las isocronas teóricas para obtener un mejor ajuste de los datos observacionales a isocronas de edad razonable. Con estos ajustes se concluye que la extinción del catálogo de [Harris \(1996\)](#) está subestimada en algunos de los cúmulos analizados. También se encuentran algunas desviaciones entre la metalicidad de la literatura y la aquí ajustada. Concluimos que no es posible determinar la metalicidad y la edad de una manera precisa con este método, puesto que existen diferentes combinaciones de los parámetros que pueden dar un buen ajuste de las isocronas al DCM observado.

Para el análisis del método de cálculo de la HFE, se crean poblaciones estelares sintéticas a partir de los modelos de evolución estelar que simularán datos observacionales reales. Así, es posible comparar las HFEs conocidas de las poblaciones sintéticas con las obtenidas por el método. Se crean poblaciones de varias maneras: i) utilizando un diagrama sintético construido con una rango amplio de edad y metalicidad y seleccionando estrellas viejas a) en un rango fijo de edad y metalicidad (selección rectangular), y b) asignándoles una probabilidad gaussiana dependiendo de su metalicidad y edad (selección gaussiana). En este caso se han creado poblaciones de dos edades viejas (10 y 12 Gyr) y tres metalicidades ($[Fe/H]=-0.5, -1.0, -2.0$); ii) creando poblaciones en un rango pequeño de edad y metalicidad directamente a partir de los modelos de evolución estelar, lo que permite crear muestras con mayor número de estrellas. Así, se han creado poblaciones simples en todo el rango de edad y una única metalicidad. En ambos casos se simuló los errores observacionales típicos del *Gaia Catalog of Nearby Stars* (GCNS) ([Gaia Collaboration et al., 2021a](#)).

Se comprueba la exactitud y precisión con las que CMDft.Gaia es capaz de recuperar la HFE, en función de tres aspectos: el rango de edad de las poblaciones simples en las que se divide el diagrama madre (bin de edad), el número de estrellas en los cúmulos sintéticos y la dependencia con la metalicidad.

Se prueba con cinco conjuntos de bins de edad de diferentes tamaños. También, se prueban dos muestras de cúmulos con diferente número de estrellas. Se obtiene que aunque el número de estrellas en el diagrama sea muy pequeño (≈ 2000 estrellas por cúmulo) el método es capaz de recuperar la HFE. A partir de este número mínimo de estrellas no se ve ninguna dependencia importante en el número de estrellas del diagrama de entrada. Analizando los resultados de la HFE de estos tests se encuentra que, como era de esperar, se tiene una mejor resolución y exactitud en edad para cúmulos sintéticos jóvenes, obteniéndose una gran dependencia de la precisión con la edad del cúmulo recuperado. Además, se encuentra que la precisión y la exactitud del método depende de los bins de edad con mucha más importancia que con el número de estrellas del set de datos. Al probar con diferentes tamaños en edad de las poblaciones simples, se obtienen los bins de edad adecuados para este set de datos. Por otro lado, parece que a metalicidades menores los cúmulos se recuperan con menor precisión que a metalicidades altas. No podemos asegurar esto porque los cúmulos creados tienen menos estrellas en metalicidades bajas o están distribuidas en un rango de metalicidad más grande que para cúmulos con metalicidades altas.

2. Introduction

Analizar la evolución de las estrellas mediante datos fotométricos ha sido una técnica explorada en gran medida en la astrofísica moderna. Sin embargo, la calidad de los datos del satélite *Gaia* ha supuesto una revolución en el estudio de las estrellas de la Galaxia. Con estos datos es posible contrastar y mejorar con una precisión sin precedentes los modelos de evolución estelar. Para este fin, los cúmulos globulares son bancos de pruebas muy interesantes por ser puramente poblaciones simples de estrellas a edades viejas. Además, gracias a la calidad de los datos y al desarrollo de potentes algoritmos es factible el cálculo de la historia de formación estelar de zonas de la Vía Láctea a gran escala. Con este marco, se ponen a prueba estos algoritmos para verificar su fiabilidad y precisión en un amplio rango de edades con poblaciones sintéticas que permiten la comprensión del método en un contexto amplio.

The study of the evolution of stars has been an extensively researched topic within the realm of modern astrophysics. For this purpose, one of the most important tools are Hertzsprung-Russell diagrams (HRDs). Empirical HRDs show relationships between stellar spectral type and luminosity (Gaia Collaboration et al., 2018). When diagrams display color index (related with stellar spectral type) and absolute magnitude (instead of luminosity), they are called color-magnitude diagrams (CMDs).

The *Gaia* space mission, of the European Space Agency (ESA), has meant a revolution in the astrophysics of the Milky Way. This satellite was launched on September 2013 and plans to continue providing data until 2025¹. Its main objective is mapping $\sim 10^9$ stars in our Galaxy providing photometry, positions, proper motions and parallax, among others. Perhaps the most incredible aspect of this program is the unprecedented precision of its data, taking into account the large number of stars measured ($\sim 1\%$ of Milky Way's stars).

In this work globular clusters (GCs) are analysed using *Gaia* data. GCs are stellar systems that usually contain about 10^5 stars. They often have a spherical distribution where the center is the area with the highest stellar density (see Karttunen et al., 2017, chap 17). These objects are very old and fantastic for studying stellar evolution. Another property that characterises them is that all stars in the cluster have a very similar age and metallicity (typically defined as the amount of one chemical element relative to another, usually iron relative to hydrogen, $[\text{Fe}/\text{H}]$ ²). That is not always true, sometimes GCs have multiple populations, i.e, there are subgroups of stars with ages and metallicities somewhat different from each other (see Piotto et al., 2012). Most GCs are in the halo of the Milky Way, so large extinctions in these objects are not expected. However, distances measured by *Gaia* to these clusters are not very precise because they are far away. They have smaller parallax and have large parallax error compared for example to stars in the disc close to the Sun for which Star Formation Histories (SFHs) are being determined by the research team hosting this TFG (see Gallart et al., 2019 and Ruiz-Lara et al., 2020). A number of GCs are located in the bulge region and affected, in addition to large parallax errors, by large interstellar extinction. There are GCs in other galaxies (see Barmby & Huchra, 2001), but all the clusters analysed in this work belong to the Milky Way.

¹<https://sci.esa.int/web/gaia/>

² $[\text{Fe}/\text{H}] = \log_{10} \left(\frac{N_{\text{Fe}}}{N_{\text{H}}} \right)_{\text{star}} - \log_{10} \left(\frac{N_{\text{Fe}}}{N_{\text{H}}} \right)_{\text{sun}}$, where N_x is the x atoms number.

Stellar evolution models such as BaSTI (Hidalgo et al., 2018) or PARSEC (Bressan et al., 2012) predict the luminosity (magnitude) and temperature (color) of stars given their metallicity and age, among other parameters. That is, for a specific age and metallicity, given an initial mass function (IMF), the CMD of a star's group of given age can be theoretically calculated. An isochrone in this context is a theoretical model that represents the expected distribution of stars of a specific age and metallicity in a CMD. By comparing the observed CMD with the predicted distribution in the isochrone, it is possible to estimate the age and metallicity of a population of stars, as well as investigate the properties of their IMF. The isochrone is a fundamental tool in the study of stellar populations and their evolution over time.

The SFH of a stellar system tells us how much stellar mass, with what metallicity and when it becomes stars. Researchers at the Instituto de Astrofísica de Canarias (IAC) and University of La Laguna (ULL) have successfully developed a method to obtain SFH from photometric information, specifically from CMDs (Aparicio & Gallart, 2004 and Aparicio & Hidalgo, 2009). This method essentially computes CMDs from models of stellar evolution. Then it performs a linear combination of simple stellar populations, and the weights of these combinations are adjusted so that the distribution of stars in the resulting CMD differs as little as possible from the observed CMD.

This work presents a broad approach to these concepts focusing in GCs and synthetic simple stellar populations in a range of ages and metallicities. In the case of GCs, we performed a comparison of isochrones from stellar evolution models with observed CMDs and calculated the SFH of some synthetic clusters. GCs are very interesting objects to analyse the proper performance of stellar evolution models and SFH calculation algorithms because their ages and metallicities are very well studied and delimited by other methods, which allows a faithful comparison of theoretical knowledge with reality. Synthetic populations in a range of ages and metallicities allowed us to study the performance of the SFH calculation algorithms in a wider context.

3. Goals

Los objetivos de este trabajo son:

- i*) Determinar posibles desacuerdos entre las predicciones de los modelos de evolución estelar (BaSTI y PARSEC) y los datos observacionales en las bandas de *Gaia* comparando isocronas con diagramas color-magnitud de cúmulos globulares. Se han estimado las edades y metalicidades de estos cúmulos, en ocasiones determinando pequeñas correcciones en la extinción y en la metalicidad que se encuentra en la literatura para cada cúmulo.
- ii*) Analizar la fiabilidad del algoritmo de cálculo de la historia de formación estelar, evaluando la precisión en la determinación de edades y metalicidades. Para ello se han utilizado:
 - a*) Cúmulos sintéticos viejos de diferentes metalicidades en los que se han simulado errores observacionales estimados en un entorno local (hasta 200 pc del Sol).
 - b*) Cúmulos simulados en todo el rango de edad y metalicidad solar que también simulan un entorno local (hasta 200 pc del Sol).

This work has some principal goals. On the one hand, it aims to compare isochrones with observed CMDs of GCs from *Gaia* data, making it possible to determine possible mismatches at old ages in a range of metallicities of 2 stellar evolution libraries (BaSTI and PARSEC) as well as systematic differences between both models. In addition age, metallicity and extinction in the line of sight of the clusters will be estimated and compared with the literature. On the other hand, the accuracy and precision of the powerful algorithms to determine the SFH is analyzed. For this, some synthetic data sets created from stellar evolution models are used. Specifically, old globular clusters with different metallicities and clusters in the whole age range with solar metallicity are simulated. This will allow a better understanding of the SFH calculation method. In particular, these data will simulate a local environment (< 200 pc from the Sun).

This analysis in *Gaia* bands is relatively new and it is also useful to better understand the scope of *Gaia* data quality, especially the early installation of the third *Gaia* data release (*Gaia* EDR3) in [Gaia Collaboration et al. \(2021b\)](#).

4. The Data

All data used in this work, both observational and theoretical, are presented in this section.

4.1. Observational data

En este trabajo se usan los datos para cúmulos globulares del catálogo de [Vasiliev & Baumgardt \(2021\)](#) basados en observaciones de *Gaia*. Se toman en primera instancia parámetros del catálogo de [Harris \(1996\)](#) y se complementan con datos más actuales encontrados en la literatura. El catálogo de [Harris \(1996\)](#), aunque sea algo antiguo, es aún una herramienta de referencia muy útil. A partir de una muestra de 170 cúmulos globulares, se hace un filtrado para solo analizar en profundidad una muestra de 10 cúmulos. Para las distancias es importante recalcar que se usa un catálogo ofrecido por [Baumgardt & Vasiliev \(2021\)](#) en donde se calculan las distancias a 162 cúmulos globulares combinando distintos métodos y resultados encontrados en la literatura, obteniendo así medidas de distancias bastante precisas y en concordancia con la literatura. En cuanto a la metalicidad de los cúmulos se comparan tanto las proporcionadas por [Harris \(1996\)](#) como las encontradas en la literatura más reciente. Por último, la extinción se obtiene a partir del catálogo de [Harris \(1996\)](#) y de NASA/IPAC Extragalactic Database (NED). Se comparan ambos catálogos para los cúmulos seleccionados.

4.1.1. Source catalogue with photometric, astrometric and membership probabilities. Clusters selection

To study GCs, in this work we use a catalog developed by [Vasiliev & Baumgardt \(2021\)](#) based on data from *Gaia* Early Data Release 3 (EDR3). It includes 170 clusters with the following information:

- *Gaia* source ID
- Celestial Coordinates
- Coordinates centered on the cluster
- Parallax corrected for zero-point offset using [Lindgren et al. \(2021\)](#) (ϖ)
- Proper motion (PM)
- Parallax uncertainty
- Proper motion uncertainty
- Correlation coefficient between the two proper motion uncertainties
- G band magnitude (G)
- $G_{BP} - G_{RP}$ (color)
- Source density (stars per arcmin²)
- Quality flag (determines the number of parameters available for that source and if it has passed all quality filters)
- Cluster membership probability (MP)

This catalog has all the stars measured by *Gaia* in the field of each cluster. Therefore, to disentangle the stars of the cluster from the others in the line of sight, a membership probability (MP) is given in the catalog. To get this probability for each star, [Vasiliev &](#)

Baumgardt (2021) retrieve all sources from the *Gaia* archive located within a certain radius from the center of the cluster, adjusting this radius individually for each cluster. Then, they use the recommendations of Fabricius et al. (2021) to obtain the sources with a good quality astrometry. They show that stars brighter than $G = 13$ have fewer measured parameters, and are affected by offsets in parallax and proper motions. After, they run a complex algorithm where using proper motions, parallaxes and angular distances from the cluster center, they calculate a membership probability for each star.

An example of photometric information given by Vasiliev & Baumgardt (2021) is shown in figure 1. It is noted that the figure represents apparent magnitudes uncorrected of galactic extinction. It is very important for our analysis to work with absolute magnitudes since with apparent magnitudes the brightness will strongly depend on the distance to the star, making it incomparable with the theoretical isochrones. As a demonstration of the method, a cluster (NGC 104) will be shown as an example of all the analysis made in this work. However all figures for the 10 selected clusters will be presented in the Appendix A.

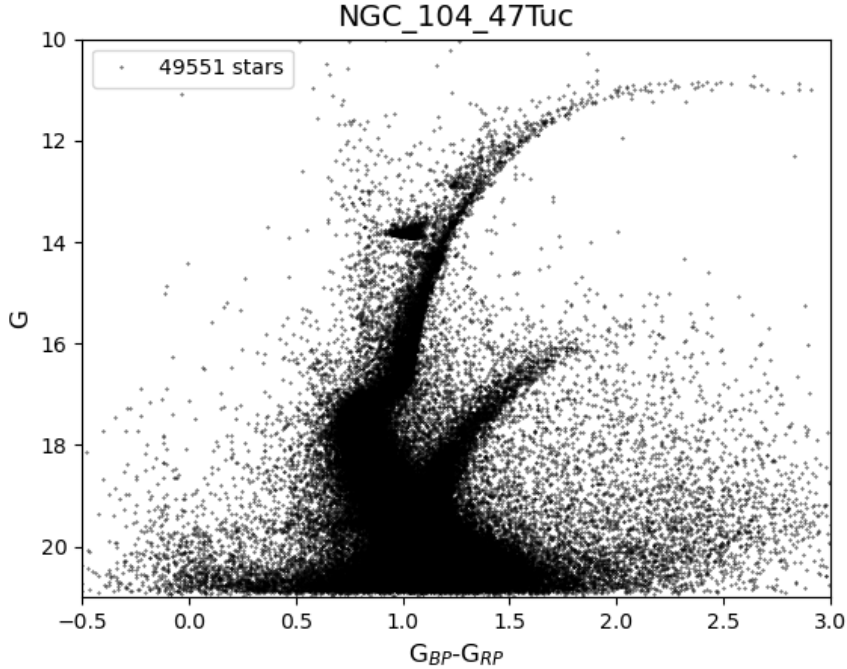


Figure 1: CMD of the globular cluster NGC 104 using apparent magnitudes in *Gaia* bands. The number of stars shown in the diagram is included. Not all of them are cluster stars, as a large part of them are stars located between the cluster and the Solar System in the line of sight towards the cluster.

After examining the data of 170 globular clusters, this work focuses on a sample of 10 GCs (Table 1). These clusters have been chosen with the following criteria:

- A wide range of metallicities needs to be covered because the shape of the isochrones depends on the metallicity of the stellar population and we want to know the behaviour of the models in the widest possible range of application. We choose clusters with the range from $[\text{Fe}/\text{H}] = -2.31$ until $[\text{Fe}/\text{H}] = -0.72$ since there are practically no known GCs beyond these metallicities.
- Clusters with low extinctions are preferably selected.
- There is also a preference for the closest clusters, thus minimizing errors in the distance measurement. The analysis of clusters beyond 12 kpc has not been considered.

GC Name	d_{\odot} [kpc]	E(B-V) [mag]	Metallicity [dex]
NGC_104	4.5	0.04	-0.72
NGC_5904	7.5	0.03	-1.29
NGC_6205	7.1	0.02	-1.53
NGC_6218	4.8	0.19	-1.37
NGC_6341	8.3	0.02	-2.31
NGC_6362	7.6	0.09	-0.99
NGC_6397	2.3	0.18	-2.02
NGC_6752	4.0	0.04	-1.54
NGC_6809	5.4	0.08	-1.94
NGC_7099	8.1	0.03	-2.27

Table 1: Selected clusters with the distance to the sun (d_{\odot}), extinction in color and metallicity by [Harris \(1996\)](#). Note that the distances, extinctions and metallicities shown here are indicative, and it will be discussed later whether they are accurate enough for this study.

4.1.2. Distances to clusters

In GCs, that are in general far away compact objects, one can adopt a single distance for all the stars in the cluster. Although the distance to the cluster can in principle be obtained from the parallax measured by *Gaia*, parallax measurements for such distant objects are not accurate enough to be used for the purpose of this work. But for academical purposes, this will be analysed below, where it will be shown how these distances would be calculated, and they will be compared with the distances available in the literature.

First, the distances (d) for each star obtained from the parallax (ϖ [mas]) measured by *Gaia* are analyzed ($d = 1/\varpi$ [pc]). Since the clusters in our sample are quite far away, the *Gaia* parallaxes are not very precise. Considering this, the stars with best measured parallaxes are selected. Only stars with parallax over parallax error greater than 5 are chosen. Therefore, only stars with parallax error equal or less than 20% are taken into account (see [Rivero et al., 2022](#) and [Andrae et al., 2018](#)).

Figure 2 shows a graph representing parallax over parallax error versus star distance to the Sun for NGC 104. The magenta line in the figure represents the distance calculated by [Baumgardt & Vasiliev \(2021\)](#) and the orange one represents the weighted average distance calculated from the *Gaia* parallaxes. [Baumgardt & Vasiliev \(2021\)](#) used some methods to calculate distances to clusters. Some of these methods are directly by parallax, or by fitting nearby stars to the main sequence of the cluster or by combining velocity dispersion profiles from *Gaia* and velocity dispersion profiles taken by HST, among others. They find distances in great agreement with the literature and with relatively low uncertainties. Distances to each cluster are calculated by averaging these methods. Essentially, data from EDR3 are combined with distances based on Hubble Space Telescope (HST) data and distances found in the literature.

To calculate the distance to the cluster by parallax, an error weighted average (equation 1) of the selected stars with relative low errors is made (see [Taylor & Thompson, 1982](#), chap 7).

$$\sigma_i = \frac{\Delta\varpi_i}{\varpi_i^2}, \quad d_{\odot} = \frac{\sum d_i \left(\frac{1}{\sigma_i}\right)^2}{\sum \left(\frac{1}{\sigma_i}\right)^2} = \frac{\sum \frac{1}{\varpi_i} \left(\frac{\varpi_i^2}{\Delta\varpi_i}\right)^2}{\sum \left(\frac{\varpi_i^2}{\Delta\varpi_i}\right)^2} \quad (1)$$

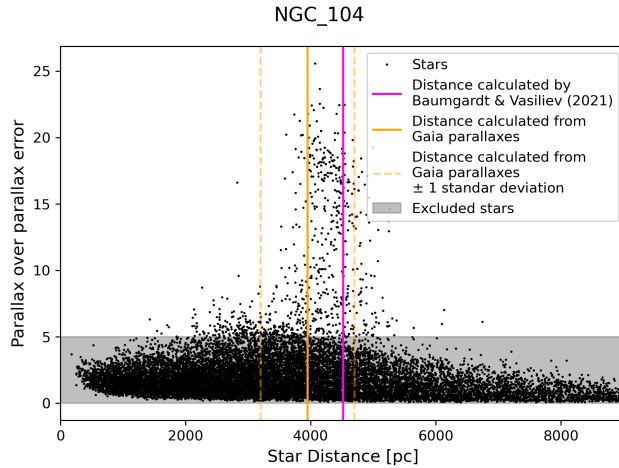


Figure 2: Parallax over parallax error versus star distance to the sun of stars of NGC 104. The magenta line represents the distance calculated by [Baumgardt & Vasiliev \(2021\)](#) and the orange one represents the weighted averaged distance calculated here from the *Gaia* parallaxes and their standard deviations.

It can be seen in Figure 2 how for the higher quality measurements the parallax distance is in agreement with [Baumgardt & Vasiliev \(2021\)](#) but even so there is a significant dispersion (in some cases the dispersion exceeds 50% of the value of the measurement). There are also appreciable shifts of the mean distance with parallax with respect to [Baumgardt & Vasiliev \(2021\)](#). In all cases, the distance calculated by parallax tends to be underestimated compared to [Baumgardt & Vasiliev \(2021\)](#) distance. In other words, it is observed that the *Gaia* parallaxes are biased towards higher values.

Since the size of the cluster is smaller than the distance dispersion of its stars, as measured by their individual parallaxes, it is more reliable and precise to use unique distances for all the stars of the cluster. Distances calculated by [Baumgardt & Vasiliev \(2021\)](#) are more recent than the [Harris \(1996\)](#) catalog and take into account many methods for calculating the distance and its error, giving this work a lot of robustness. Table 2 shows the distances that are provided in the [Harris \(1996\)](#) catalog, in [Baumgardt & Vasiliev \(2021\)](#) with their differences and the weighted average distance calculated in this work from *Gaia* parallaxes.

GC Name	d_{\odot} (Harris) [kpc]	d_{\odot} (Baumgardt) [kpc]	d_{\odot} (Parallax) [kpc]	Differences between literature catalogs [kpc]	Differences between Baumgardt and parallax [kpc]
NGC_104	4.5	4.52 ± 0.03	3.9 ± 0.7	0.02	0.62
NGC_5904	7.5	7.50 ± 0.06	6.1 ± 1.3	0.00	1.40
NGC_6205	7.1	7.42 ± 0.07	6.8 ± 1.5	0.32	0.62
NGC_6218	4.8	5.11 ± 0.05	4.4 ± 0.7	0.31	0.71
NGC_6341	8.3	8.50 ± 0.07	8.5 ± 1.2	0.20	0.00
NGC_6362	7.6	7.65 ± 0.07	6.7 ± 1.0	0.05	0.95
NGC_6397	2.3	2.48 ± 0.02	1.8 ± 0.4	0.18	0.68
NGC_6752	4.0	4.12 ± 0.04	3.5 ± 0.7	0.12	0.62
NGC_6809	5.4	5.35 ± 0.05	4.5 ± 0.7	0.05	0.85
NGC_7099	8.1	8.46 ± 0.09	5.5 ± 1.4	0.36	2.96

Table 2: Distances obtained by [Harris \(1996\)](#), by [Baumgardt & Vasiliev \(2021\)](#) and the average distances from *Gaia* parallaxes and their standard deviations. Differences between literature catalogs are included. Also, the differences between [Baumgardt & Vasiliev \(2021\)](#) and parallax distances are shown.

4.1.3. Metallicities of globular clusters

For the isochrone analysis it is crucial to know the metallicity of the clusters. In order to get the most up-to-date data, the metallicity provided by [Harris \(1996\)](#) is not enough. Therefore, the metallicity of each GC is sought individually to obtain a recent and higher quality measurement.

GC Name	Metallicity (Harris) [dex]	Metallicity (Lit.) [dex]	Literature Reference
NGC_104	-0.72	-0.81 ± 0.02	Sakari et al. (2013)
NGC_5904	-1.29	-1.19 ± 0.05	Horta et al. (2020)
NGC_6205	-1.53	-1.46 ± 0.04	Horta et al. (2020)
NGC_6218	-1.37	-1.26 ± 0.03	Horta et al. (2020)
NGC_6341	-2.31	-2.22 ± 0.03	Horta et al. (2020)
NGC_6362	-0.99	-1.07 ± 0.01	Massari et al. (2017)
NGC_6397	-2.02	-2.02 ± 0.04	Horta et al. (2020)
NGC_6752	-1.54	-1.47 ± 0.03	Horta et al. (2020)
NGC_6809	-1.94	-1.75 ± 0.04	Horta et al. (2020)
NGC_7099	-2.27	-2.31 ± 0.05	Mucciarelli & Bonifacio (2020)

Table 3: Metallicity for each cluster that is obtained from the [Harris \(1996\)](#) catalogue and from the literature.

Table 3 lists the metallicity found in the [Harris \(1996\)](#) catalog and in the literature for each cluster. In the following we include some notes regarding the literature metallicity measurements.

[Sakari et al. \(2013\)](#) obtain the metallicity of NGC 104 by high resolution spectroscopy using the du Pont echelle at Las Campanas. The spectra has been obtained using only stars in the core of the cluster.

In [Massari et al. \(2017\)](#), they measure the metallicity of the cluster based on 11 stars in the

red giant branch (RGB). They use high resolution spectroscopy measured by FLAMES on the Very Large Telescope (VLT).

In [Mucciarelli & Bonifacio \(2020\)](#), they analyze stars in the RGB of 16 GCs using spectroscopic and photometric measurements. They come to the conclusion that their spectroscopic measurements are not reliable for metal poor giant stars and they have to use the photometric measurements. So for the low metallicity cluster NGC 7099, isochrones are fitted to find its metallicity.

In [Horta et al. \(2020\)](#), they measure the metallicities of stars in multiple clusters using the 16 data release (DR16) of the SDSS/APOGEE survey and then calculate an average to obtain the metallicity of each cluster. They use kinematic parameters and the metallicities from [Harris \(1996\)](#) to select the cluster members.

4.1.4. Extinction

In addition to knowing the distance, it is necessary to determine the extinction in the direction of the cluster. Although these clusters are generally located in the halo of the Milky Way and are not significantly affected by the extinction found in the Galaxy’s disk, even small differences between the extinction values can cause noticeable displacements in the CMDs.

The extinction, in addition to the [Harris \(1996\)](#) database, is obtained from NASA/IPAC Extragalactic Database (NED)³ that is a search tool of the characteristics of astronomical objects, including extinction.

In [Table 4](#) we display the extinction values provided by [Harris \(1996\)](#) and those provided by NED. It is found that the relative difference between catalogs is significant in many cases, such as for NGC 6809. Since we do not know which one is best, we will use [Harris \(1996\)](#) as a starting point for the isochrones fitting, even though it is older. However, in [section 5.3.2](#), each cluster will be individually fit to a determined metallicity and extinction.

GC Name	E(B-V) (NED) [mag]	E(B-V) (HARRIS) [mag]
NGC_104	0.033	0.04
NGC_5904	0.032	0.03
NGC_6205	0.015	0.02
NGC_6218	0.155	0.19
NGC_6341	0.020	0.02
NGC_6362	0.067	0.09
NGC_6397	0.165	0.18
NGC_6752	0.049	0.04
NGC_6809	0.120	0.08
NGC_7099	0.045	0.03

Table 4: Color excess for each cluster for 2 catalogues, NED and [Harris \(1996\)](#).

³The NASA/IPAC Extragalactic Database (NED) is operated by the Jet Propulsion Laboratory, California Institute of Technology, under contract with the National Aeronautics and Space Administration. <https://ned.ipac.caltech.edu/>

4.2. Synthetic data

Con el fin de comprobar la precisión del método de cálculo de la SFH, además de verificar el comportamiento de los distintos parámetros modificables del método, se crean cúmulos sintéticos en todo el rango de edad (desde 12 Gyr hasta 20 Myr). Estos cúmulos de estrellas sintéticas usando creados por modelos de evolución estelar y se seleccionan sus miembros de diferentes maneras. Estos sets de datos pretenden simular poblaciones estelares simples en un entorno local (hasta 200 pc del Sol).

4.2.1. Synthetic clusters at old ages

The SFH calculation method (Gallart et al. in prep) developed by the team hosting this TFG is being tested and its performance is being evaluated. In this work we performed tests using synthetic clusters to understand the effects of the code's parameters on the derived SFH and to determine the precision and accuracy of the method. These synthetic clusters are composed of stars in a certain small age and metallicity range. They are created selecting stars from an artificial set (which will be referred to as the mother diagram from now on) that has been generated using stellar evolution models. This synthetic set of stars includes information such as their magnitude, color, age and metallicity.

The technique of selecting these synthetic clusters is important because the aim is to simulate what would be found with real data, such as clusters of stars with unique ages and metallicities. Hence, 2 methods of selecting these populations are tested. Their SFHs will be calculated as described in section 5.4 and the results will be described in section 6.5.

The first method selects all the stars within a given range of metallicity and age in the synthetic set of stars (that we are calling mother CMD). This technique is hereinafter called rectangular selection.

The second technique involves assigning a 2 dimensional Gaussian probability (in terms of age and metallicity) with a given sigma, centered on a certain metallicity and age. The probability of each star in the mother diagram ($P(i)$) of being chosen depends on its age and metallicity in the following rescaled space:

$$p_i = e^{-1/2 \left[\left(\frac{[\text{Fe}/\text{H}]_i - [\text{Fe}/\text{H}]_{center}}{\sigma_{[\text{Fe}/\text{H}]}} \right)^2 + \left(\frac{\text{age}_i - \text{age}_{center}}{\sigma_{age}} \right)^2 \right]} \quad (2)$$

$$P(i) = \frac{p_i}{\sum_i^{N_{stars}} p_i} \quad (3)$$

This rescaling is done because it is not appropriate to define distances in the age-metallicity space to assign probabilities. Therefore, a rectangle is selected in this space from which it is rescaled. That is, the space is transformed linearly to one in which the (0, 0) and (1,1) points in this new space are the limits of the rectangle in the age-metallicity plane. N stars are selected from the mother diagram (if there is enough) with the above gaussian probability. This technique is hereinafter called Gaussian selection.

These 2 techniques are used to select six synthetic GCs, three at 10 ± 0.02 Gyr and three at 12 ± 0.02 Gyr. Each one of the three synthetic GCs will have a different metallicity: $[\text{Fe}/\text{H}] = -0.5 \pm 0.05$, $[\text{Fe}/\text{H}] = -1.0 \pm 0.05$ and $[\text{Fe}/\text{H}] = -2.0 \pm 0.05$. Here $\pm x$ means, in the case of rectangular selection, the width in age (or metallicity) of the cluster and for the Gaussian selection it means the sigma of the Gaussian ($\sigma_{[\text{Fe}/\text{H}]}$ and σ_{age}) used to assign probabilities to each star of being selected.

Figures 3 and 4 display the number of stars selected for each age and metallicity, along with a CMD and the characteristics of the two selections (rectangle and Gaussian) for one age (10 Gyr). The selections have been done using a mother diagram of 120 million stars in which photometric and distance errors are simulated to mimic a sample of stars within 200 pc of the Sun. 10000 stars were requested for each synthetic cluster (a number not always achieved)

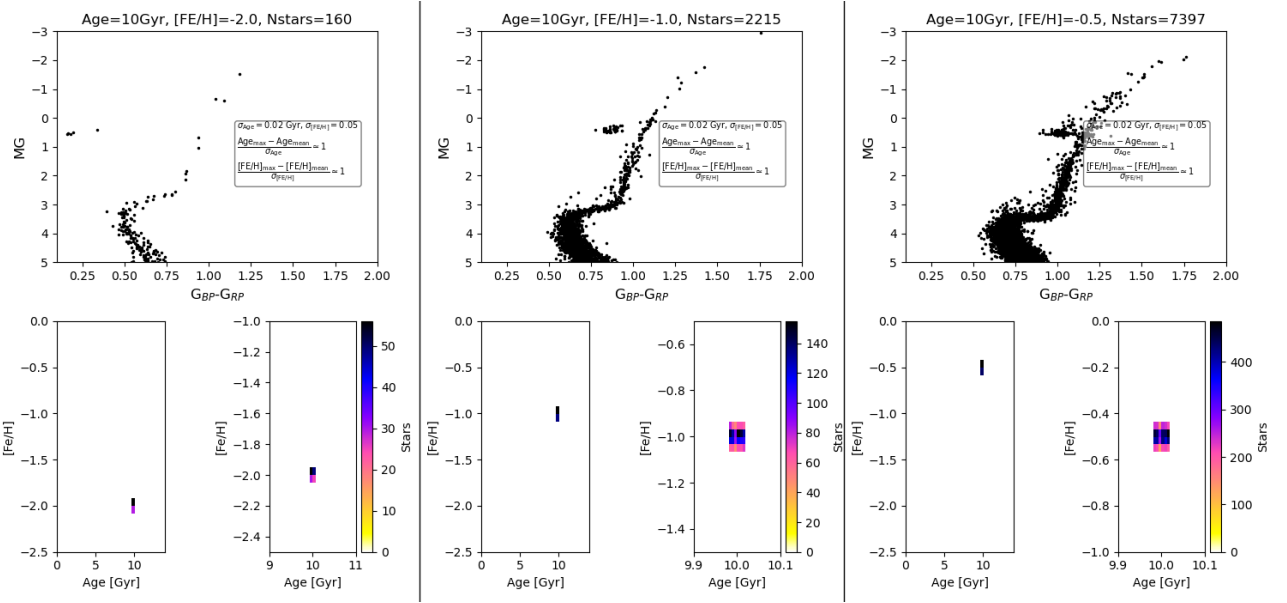


Figure 3: CMD of the three synthetic GCs of 10 Gyr selected by the rectangle selection. A 2D histogram of the selected stars in the age-metallicity plane is also included.

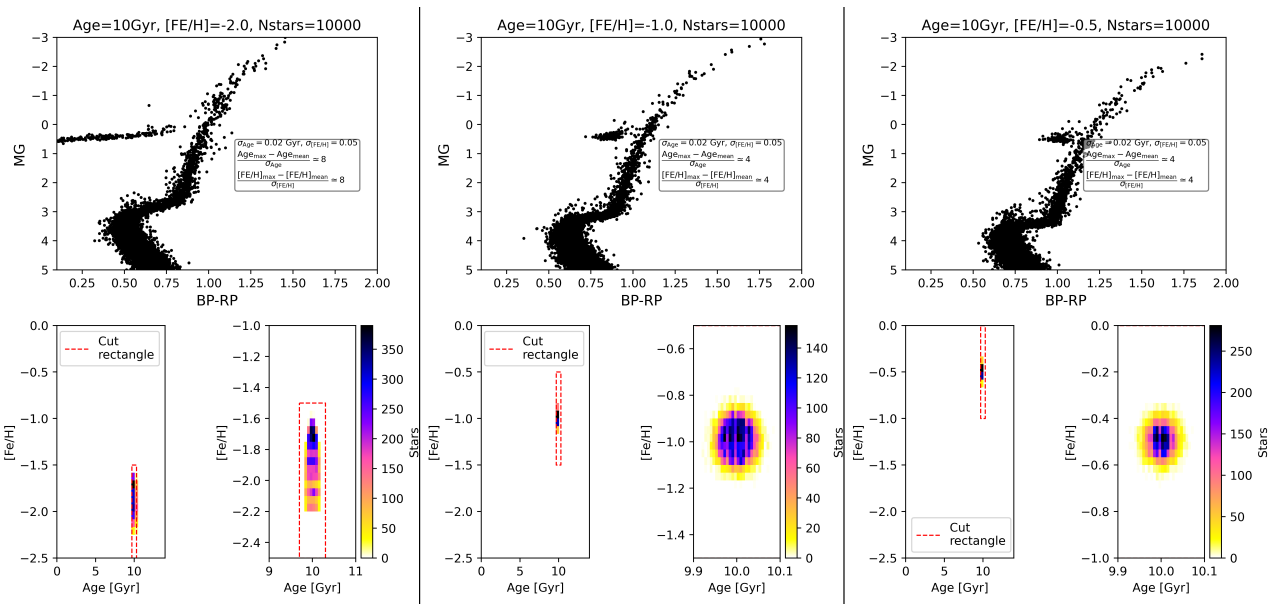


Figure 4: CMD of the three synthetic GCs of 10 Gyr selected by the Gaussian selection. A 2D histogram of the selected stars in the age-metallicity plane is also included. The cut rectangle is used for the rescaled space.

It should be noted that in the most metal poor cluster, in the Gaussian selection, the selected stars do not follow a Gaussian of the given sigma, because there are not enough stars in the mother CMD with ages and metallicities close to the central age and metallicity. So to get 10000 members, stars with very low probabilities are chosen.

4.2.2. Synthetic clusters at all ages

In addition of testing the SFH calculation method at old ages and different metallicities, it is important to know how the method performs at young and intermediate ages (since the CMD is quite different between young and old stellar populations). For this purpose, stars are selected from a synthetic CMD created for each population in order to have sufficient number of stars at one metallicities ($[\text{Fe}/\text{H}] = -0.1 \pm 0.05$) and at 0.2 ± 0.02 , 2 ± 0.02 , 4 ± 0.02 , 6 ± 0.02 , 8 ± 0.02 , 10 ± 0.02 and 12 ± 0.02 Gyr. Here, again $\pm x$ refers to the total width of the stellar population in age and metallicity, that is, 20 Myr in age and 0.05 dex in metallicity. Photometric and distance errors are simulated to mimic a nearby sample.

It will also be interesting to check the performance of the SFH calculation method according to the number of stars in the observed CMD, so the selection in the previous paragraph will be done by selecting for the final CMD 15000 and 100000 stars. An input CMD are shown in Figure 20. The difference of each population in the CMD as age changes is clear, showing the need to test across the whole age range and not just focus on older ages.

5. Methodology

5.1. Transformation to the absolute magnitude plane

Es necesario transformar los diagramas color magnitud a magnitudes absolutas para comparar con las isocronas teóricas y que no haya una dependencia con la distancia en estos diagramas. Por otro lado, se corrige la extinción interestelar usando una serie de expresiones que relacionan el exceso de color $E(B-V)$ en los filtros Johnson con la extinción en el sistema fotométrico de *Gaia*.

Distance is the key to transform the data to the absolute magnitude plane. Only in absolute magnitude is possible to compare the CMD with theoretical isochrones. To convert to the absolute magnitude plane, [Baumgardt & Vasiliev \(2021\)](#) distances are used, as previously justified. To do this, the equation 4 (expressed for the Gaia band G) is applied.

$$M_G = G + 5 - 5 \log (d [\text{pc}]) - A_G \quad (4)$$

Where M_G is absolute magnitude, G is apparent magnitude, d is the distance to the star in parsec and A_G is the extinction correction.

To calculate the extinction correction for each star, it is necessary to know the color excess, $E(B-V)$, and effective temperature of the star (T_{eff}). The following relationships (equations 5) are used to obtain the extinction corrections ($A_G, A_{BP}, A_{RP}, E_{BP-RP}$). These relationships are the same ones used by [Rivero et al. \(2022\)](#) in her TFG work. T_{eff} is obtained from the star's color using the relationship provided by Tomás Ruiz Lara in a private communication. Then, color is corrected with the calculated extinction and the effective temperature is recalculated. This process is repeated for each star iteratively 10 times for good convergence.

$$\begin{aligned} T_{eff} &= 62.55257114(G_{BP} - G_{RP})_0^4 - 975.10845442(G_{BP} - G_{RP})_0^3 + \\ &\quad + 4502.86260828(G_{BP} - G_{RP})_0^2 - 8808.88745592(G_{BP} - G_{RP})_0 + 10494.72444183 \\ A_G &= (1.4013 + T_{eff} \cdot (3.1406 - 1.5626 \cdot T_{eff})) \cdot E(B-V) \\ A_{BP} &= (1.7895 + T_{eff} \cdot (4.2355 - 2.7071 \cdot T_{eff})) \cdot E(B-V) \\ A_{RP} &= (1.8593 + T_{eff} \cdot (0.3985 - 0.1771 \cdot T_{eff})) \cdot E(B-V) \\ E_{BP-RP} &= A_{BP} - A_{RP} \\ (G_{BP} - G_{RP})_0 &= G_{BP} - G_{RP} - E_{BP-RP} \end{aligned} \quad (5)$$

5.2. Cluster members selection

Para limpiar el CMD de estrellas que no pertenecen a los cúmulos se excluyen todas las estrellas con *membership probability* (MP) < 0.9 debido a que la distribución de estrellas según su MP está claramente dividida en 2, una porción con probabilidades bajas ($< 20\%$) y el resto con probabilidades muy altas ($> 80\%$). Aún así, el CMD no es todo lo estrecho que se espera

de un cúmulo globular. La razón más probable de esto son los altos errores en la medida de las magnitudes de las estrellas debido a la gran densidad estelar (o crowding), en las zonas centrales del cúmulo. Para seleccionar las estrellas con las mejores medidas fotométricas se ajusta una gaussiana en 2 dimensiones a la distribución estelar en el plano del cielo. A partir del ajuste se crea una elipse, y todas las estrellas que se encuentren en su interior no se toman en cuenta.

As seen in figure 1, there are many stars that do not belong to the clusters in the observed CMDs. For discerning which ones belong to the clusters, membership probabilities (MP) provided by Vasiliev & Baumgardt (2021) are utilized, as explained in section 4.

Only stars with $MP > 0.9$ are chosen. This is because when looking at a histogram of the MP of each cluster (Figure 5), there are two peaks and it seems that all the stars not belonging to the cluster have $MP < 0.2$, always finding a peak from 0.9 (corresponding to the own stars of the cluster). We also tried to clean the CMD by choosing only stars with $MP > 0.99$ but there is no significant change in the quality of the CMD. So to increase the number of stars in the CMD, 0.9 is definitely chosen as a cut.

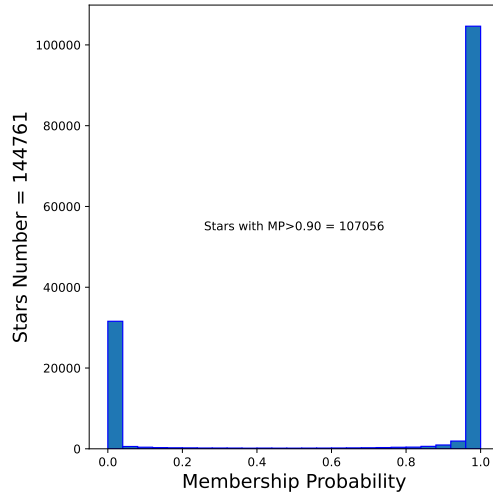


Figure 5: Histogram of the membership probabilities for NGC 104.

On the other hand, the CMDs of GCs are expected to be narrow because stars of a GCs have the same age and chemical composition. However, this is not always the case for several reasons. One of them are unresolved binary systems, which can widen the main sequence. Additionally, due to the fact that the centers of these clusters tend to be very dense and populated, *Gaia* may have difficulties in observing the magnitudes and colors of individual stars, as the light of different stars can overlap and introduce errors. This effect is known as crowding.

In order to remove from the CMD the stars close to the center of the cluster affected by large errors due to crowding, a two-dimensional Gaussian is fitted to the star distribution in the sky plane for each cluster using a nonlinear least-squares method (this is applied only to stars with $MP > 0.9$). This produces two Gaussian sigmas, one for each axis. Then, stars within an ellipse where each semiaxis is a multiple (hereafter `mul_sigma`) of each sigma calculated by the fit are excluded. This removes all central stars from the CMD. A value of 2 is used as `mul_sigma` in each axis to remove the central stars, as this value provides a good cleaning of the CMD for all clusters.

It is not expected to introduce any significant bias in the CMD by removing all central stars from the cluster. This is because we do not expect strong radial relations in the distribution of ages and metallicities of the stars, but rather a very uniform distribution that is characteristic of an almost simple stellar population.

Figures 6 and 7 show the star distribution in the sky plane with the fitted Gaussian overlaid and the cutting ellipse (excluding all stars inside to avoid crowding) created using `mul_sigma` and the fitted sigmas. Figure 7 shows the fitted Gaussian in 3D and the cutting ellipse.

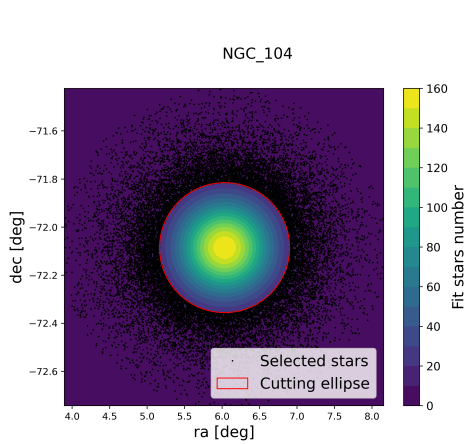


Figure 6: Star distribution of NGC 104 in the sky plane. The fitted Gaussian is overlaid together with the cutting ellipse (which is created using `mul_sigma` and the fitted sigmas).

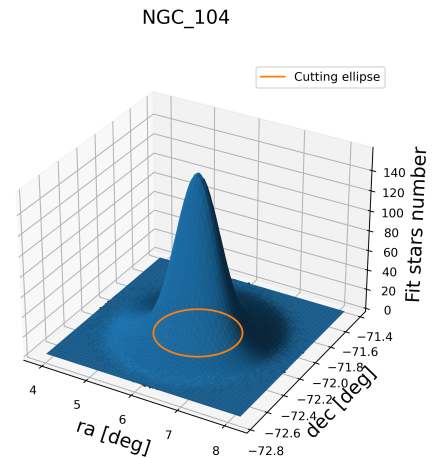


Figure 7: Fitted Gaussian with the star distribution of NGC 104 in the sky plane.

Figure 8 shows an example of the NGC 104 CMD cleaned in this way. Stars with $MP < 0.9$ are shown in gray, those eliminated by the crowding ellipse are shown in red, and the stars that pass all the filters and are used for analysis are shown in black.

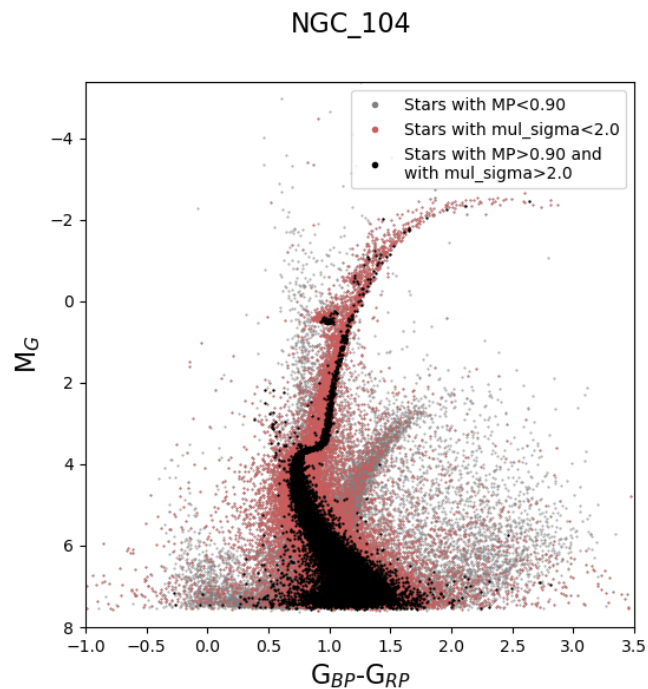


Figure 8: CMD of NGC 104 in absolute magnitude with filters applied. Stars with $MP < 0.9$ are shown in gray, those eliminated by the crowding ellipse are shown in red, and the stars that pass all the filters and are used for analysis are shown in black.

5.3. Comparison with isochrones

Se presenta una comparación entre las isocronas de los modelos BaSTI y PARSEC superponiéndolas con los CMDs de los cúmulos globulares en el plano de magnitudes absolutas (que ha sido corregido por extinción). Para las isocronas se fija una metalicidad y se crean en un rango de edades entre 11.5 Gyr y 14.5 Gyr. Debido a las diferencias sistemáticas entre los CMDs y las isocronas también se ajusta manualmente la metalicidad y extinción de cada cúmulo hasta que el CMD concuerde con unas isocronas de edad razonable.

5.3.1. Comparing between models: BaSTI and PARSEC

For each cluster a comparison between its CMD and theoretical isochrones made from stellar evolution models is performed. First of all, for each cluster, four isochrones are obtained from [Hidalgo et al. \(2018\)](#) (BaSTI⁴) and from [Bressan et al. \(2012\)](#) (PARSEC⁵). To obtain them (both stellar evolution models sets are solar scaled), the metallicity is fixed from the literature (Table 3) and the age is varied from 11.5 Gyr to 14.5 Gyr in steps of 0.5 Gyr. Ages greater than the age of the Universe are included because there are GCs CMDs that are not fit by isochrones at younger ages. This will be further discussed later. In section 6.2 the two models will be discussed.

Figure 9 shows an example of the superposition of the isochrones, using both BaSTI and PARSEC in the theoretical absolute plane. Both CMDs have been corrected by [Harris \(1996\)](#) extinction and the same metallicity from literature. The comparison of all the selected clusters with BaSTI and PARSEC isochrones is shown in appendix A.3 .

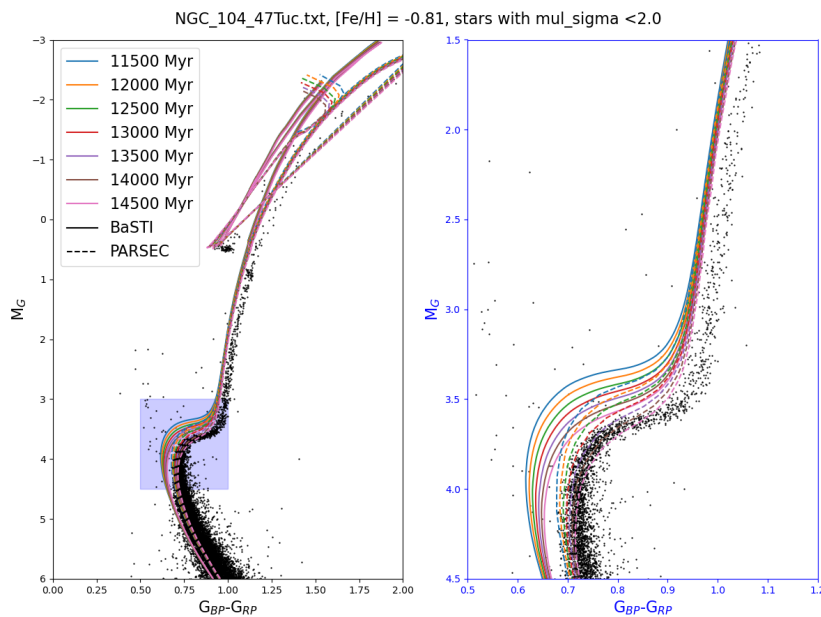


Figure 9: CMD of the extinction corrected star selection of NGC 104, overlapped with the BaSTI (continuous lines) and PARSEC (dashed lines) isochrones.

⁴BaSTI isochrones: <http://basti-iac.oa-abruzzo.inaf.it/isocs.html>

⁵PARSEC isochrones: <http://stev.oapd.inaf.it/cgi-bin/cmd>

In order to determine the age through comparison with isochrones, it is necessary to focus on the turnoff region. The turnoff is the location in the CMD where stars of a certain age and metallicity depart from the main sequence because the hydrogen in their cores has been fully consumed (see [Chiosi et al., 1992](#) and [Karttunen et al., 2017](#), chap 12).

5.3.2. Individual BaSTI and PARSEC fits

The metallicity and extinction of each cluster are manually adjusted to find the best visual fit to BaSTI isochrones with reasonable ages (also, PARSEC isochrones have been fitted for two clusters: NGC 104 and NGC 6809, Figures 15 and 17). The CMD of NGC 104 is shown in Figure 14 after applying this method (in NGC 104 corrected from $[\text{Fe}/\text{H}]=-0.81$ to $[\text{Fe}/\text{H}]=-0.60$ and maintaining the extinction) for BaSTI isochrones. The results of applying this method to all the clusters are shown in section 6.3.

5.4. The SFH calculation method

El método para calcular la SFH a partir de un CMD observado es una poderosa herramienta que se pretende probar, ver sus limitaciones, dependencia del resultado con los parámetros del método, etc. Este algoritmo calcula la combinación de poblaciones simples que mejor reproduce el CMD observado a partir de compararlo con el CMD de un gran número de combinaciones de poblaciones simples de las que se conocen las edades y metallicidades, hasta encontrar el mejor ajuste. Cada población simple tiene un peso en la población estelar final calculada, que está relacionado directamente con la masa que se convierte en estrellas de esa edad y metalicidad. De gran importancia es el tamaño en edad y metalicidad de estas poblaciones simples creadas porque es un parámetro directamente relacionado con la resolución de la solución en términos de edad y metalicidad. Este aspecto se analiza en profundidad en este trabajo. El tamaño de las poblaciones simples en edad dependerá de la propia edad de la población debido a que la distribución de estrellas en el CMD cambia de manera diferente según la edad de las poblaciones simples. Se hallan las SFHs de los cúmulos sintéticos explicados en la sección 4.2.2 para distintos tamaños en edad de las poblaciones simples. A partir de ajustar gaussianas a estos cúmulos en el plano edad-metalicidad se podrán analizar las diferencias en la precisión con que se obtienen las edades y metallicidades de los cúmulos sintéticos para distintos tamaños de las poblaciones simples.

The SFH calculation method (Gallart et al. in prep) is a powerful tool to calculate the SFH of a set of stars from just photometric measurements. Previous versions of the algorithm used in this work have produced amazing results regarding the SFH of the Galaxy ([Gallart et al., 2019](#) and [Ruiz-Lara et al., 2020](#)). The method is mainly based on the IAC-POP code ([Aparicio & Hidalgo, 2009](#)).

The method consists on comparing the CMD of the stars whose SFH is to be derived (hereafter called the observed CMD or input CMD) with a synthetic CMD with simulated observational errors from which ages and metallicities of the stars are known (hereafter called the mother CMD). Because the distributions of the stars in the CMD are not random, but there is a relation between the age and metallicity with position and number of stars in a region of the CMD, it is possible to calculate the SFH.

In essence, a CMD (called the result CMD) is calculated for which the metallicities and ages of its stars are known from comparing and minimising the differences with the observed CMD. To do this, a huge number of linear combination of simple stellar populations is created. By adjusting their weights to minimise the differences with the observed CMD, a complex stellar population very similar to the observed one can be obtained. This process gives as a result the SFH of the system, which can be defined as the mass transformed into stars per unit time and metallicity, as a function of time and metallicity. Moreover, multiple solutions are calculated and then averaged to reduce the random errors introduced by the method. Another relevant feature of this algorithm is that does not give equal importance to all areas of the CMD. First of all, it is defined which area of the complete CMD is included in the analysis, i.e. it is possible to exclude any region of the diagram for reasons like high photometric errors, low accuracy of the models (e.g. in the RGB as it is a region where the stars are in an advanced state and therefore the errors propagated can be important), etc. Then, the code assigns greater or lesser importance to each zone of the selected CMD based on its relevance in characterizing a stellar population. For example, the low brightness main sequence region will be given less weight than the bright portion because it contains many populations at any age and metallicity. On the contrary, the very bright main sequence is very characteristic of only young age populations so it will have great importance (whether there are stars or not) in calculating the solution.

To show the possibilities of the method, SFHs are calculated for the synthetic clusters explained in section 4.2.

5.4.1. Testing the bin size of the SFH calculation method

In the method there are free parameters that can be modified according to the type of input data. An important one is the width in age and metallicity of the simple stellar populations that are created (from now on it will be called age or metallicity bin). Bins size is not a trivial problem because not all simple populations should have the same size, i.e., these sizes should vary according to the age of the simple population. This is because the age resolution of the theoretical models varies with age. For example, two simple populations that differ in 1 Gyr at old ages have a distribution of stars in the CMD very similar to each other; in contrast, two simple populations that also differ in 1 Gyr at young ages have a distribution of stars in the CMD quite different (see Figure 20). Therefore, the age resolution is expected to be lower at older ages and so it is reasonable that the size of the simple populations is larger as the age is older. Furthermore, this does not follow a linear relationship. On the other hand, it would not make sense to make bins such that the difference in color or magnitude between 2 consecutive bins is similar to the error in the measurement (both photometric and due to the error in distance in the case of magnitude).

In this work, we analyze the differences and dependencies with the size of the age bins in the calculated SFH of the data sets created in section 4.2.2 (synthetic clusters in a wide age range). Tests are carried out to determine the best size of the bins for data sets with errors like GCNS⁶.

Figure 10 shows the different sets of age bins that have been tested. The ones depicted in colors (labelled `recast x`, the number x is related to the number of age bins in the whole age interval, with, for example, twice the number of bins for recast 1 compared to recast 0.5) have been constructed taking into account the varying differences in color and magnitude of

⁶Currently the *Gaia* Catalog of Nearby Stars (GCNS) (Gaia Collaboration et al., 2021a) is being analyzed with this method by the research team hosting this TFG. This catalog includes sources measured with *Gaia* inside a 100 pc sphere around the sun. It is characterized by having very good quality in the photometry as well as being very complete.

the isochrones as a function of age while the one depicted in black (linear) has a linear increase of the size of the bins as a function of age, such as the oldest age bins has a size of 1 Gyr.

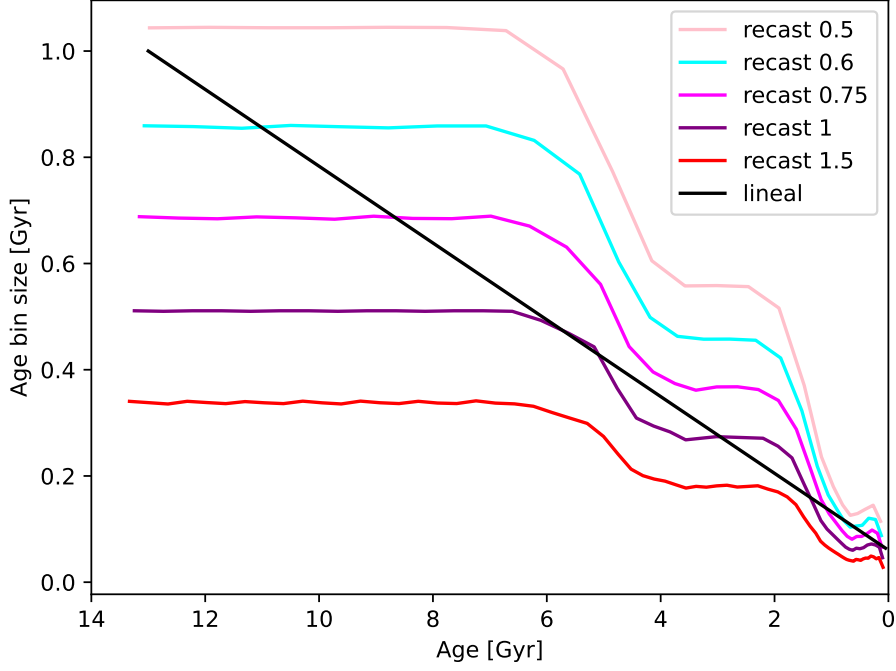


Figure 10: Age bin size as a function of age of the simple stellar populations created by the method.

SFHs have been calculated for the synthetic clusters at all ages defined in section 4.2.2. From the result CMD of each of these SFHs, a Gaussian is fitted (with a program provided by the team hosting this TFG based on the Scikit-learn python package (Pedregosa et al., 2011) using a Gaussian mixture model) to the stars in each recovered synthetic cluster in the age-metallicity plane. With the information of the center of the Gaussian and its sigmas it is possible to measure the precision and accuracy of the method. Figure 11 shows an example of how these Gaussians would fit each synthetic cluster solution in the age-metallicity plane for a particular bin size (recast 0.75) and for the input sample of 15000 stars.

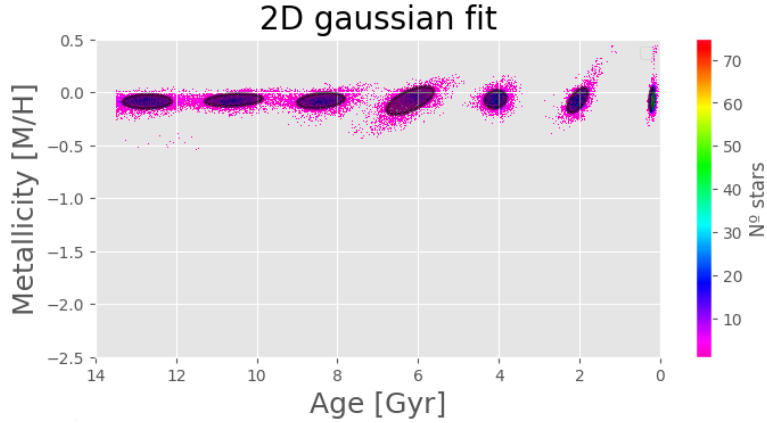


Figure 11: Solution diagram for recast 0.75 in the age-metallicity plane with the Gaussian fitted for each synthetic cluster.

6. Results

6.1. The accuracy of extinction and metallicities from the literature

Se analizan los posibles desajustes entre las isocronas y los datos de los cúmulos que son comunes a ambas librerías de modelos de evolución estelar. Esto nos ha permitido observar que hay una subestimación de la extinción en la mayoría de cúmulos globulares seleccionados, tanto usando los valores del catálogo de Harris como los de NED (Tabla 5).

Comparing the CMDs of GCs with isochrones, using the literature metallicities in Table 3 and Harris extinctions in Table 4 shows that many of the selected clusters have a systematic shift in all the CMD with respect to the theoretical isochrones as can be seen in the example in the Figure 12. This figure shows the isochrones of BaSTI (with continuous lines) and the isochrones of PARSEC (with dashed lines), as well as the stars in the CMD of NGC 6809.

Figure 9 also shows that there are no reasonable ages compatible with the CMD of NGC 104 if the metallicities and extinctions in the tables mentioned above are used. This is probably due to some inaccuracy in the metallicity calculated for this cluster since with a change of metallicity (from $[\text{Fe}/\text{H}]=-0.81$ to $[\text{Fe}/\text{H}]=-0.60$) a good fit is achieved as can be seen in Figure 14.

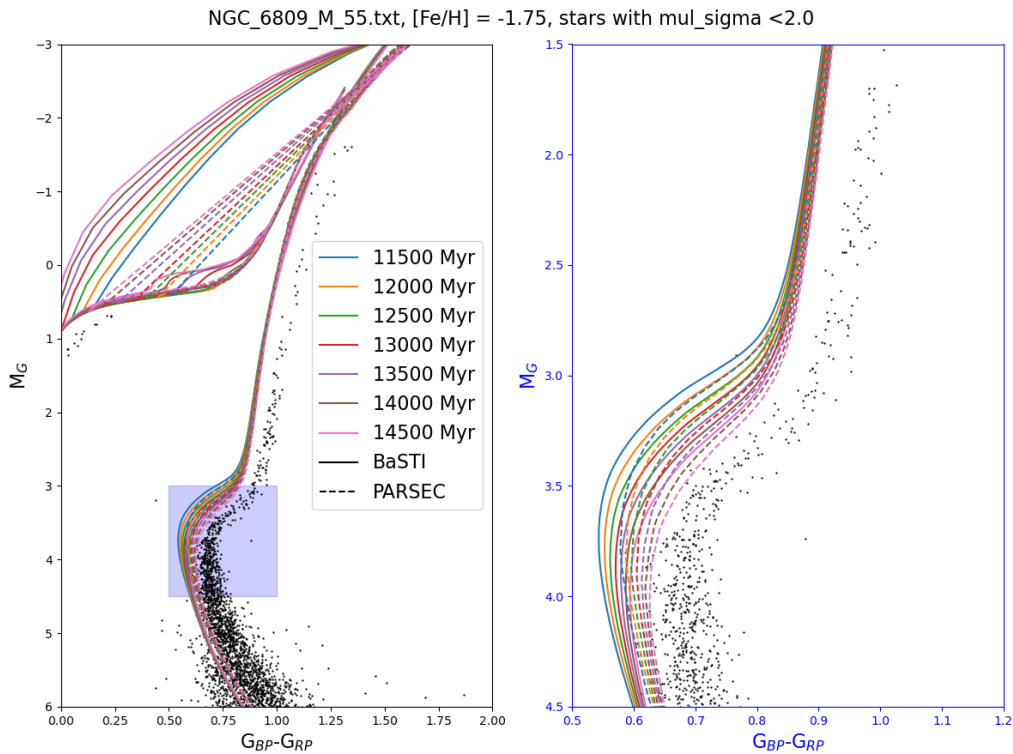


Figure 12: CMD of the extinction corrected star selection of NGC 6809, overlapped with the BaSTI and PARSEC isochrones.

6.2. Differences between the BaSTI and PARSEC stellar evolution libraries

Se encuentran diferencias entre las isocronas de BaSTI y PARSEC. Las isocronas de PARSEC son más rojas que las de BaSTI. Esto puede llegar a tener cierto impacto en la SFH, que dependería del modelo usado.

Figures 9 and 12 show that the BaSTI and PARSEC isochrones have differences in color in the main sequence at the metallicities of these two clusters. In this section we will examine this in more detail.

Figure 13 shows isochrones (BaSTI and PARSEC) in the turnoff region with three different ages and three metallicities. There are considerable differences between the two libraries. At high metallicities the differences are more noticeable. But in the whole metallicity range studied, in the main sequence and in the turnoff, the PARSEC isochrones are redder than the BaSTI isochrones. The subgiant branch is fainter in PARSEC. In contrast, the RGB has a similar color in both libraries. This means that the difference in color of the RGB and the main sequence is larger in BaSTI than in PARSEC and may result in difficulties for one of the libraries to fit the main sequence and RGB at the same time. These differences will likely lead to non-negligible differences in the SFHs derived with both models.

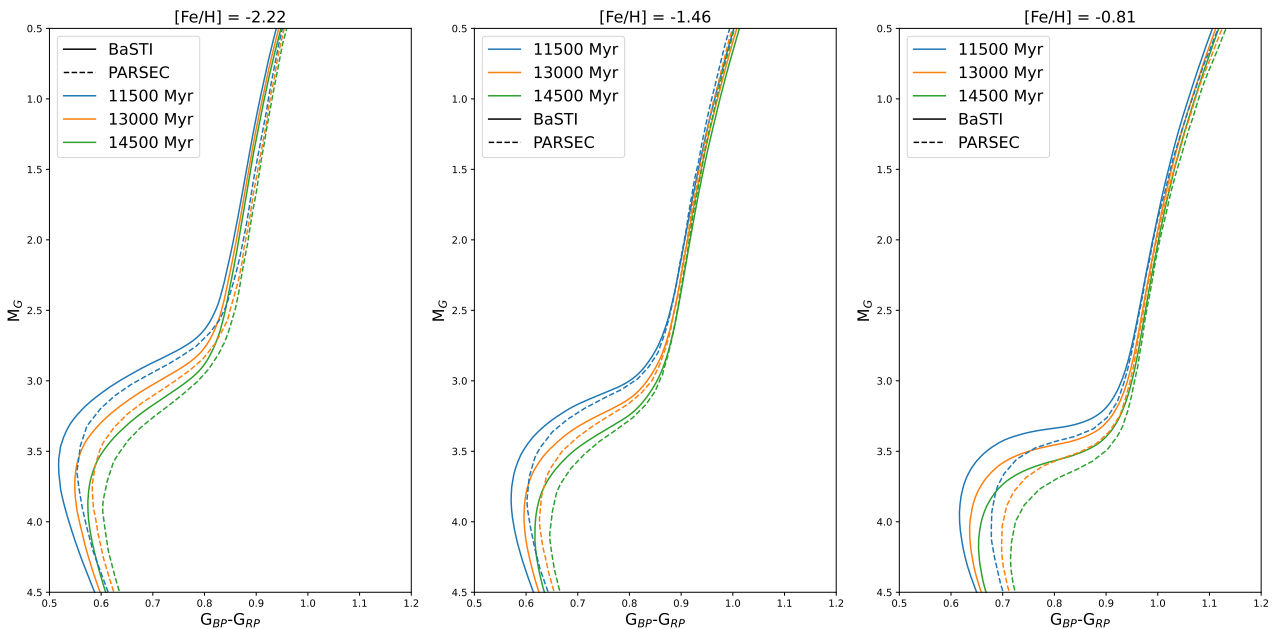


Figure 13: BaSTI (continuous lines) and PARSEC (dashed lines) isochrones with 3 different ages and 3 metallicities, focused on the turnoff region.

6.3. Individual BaSTI and PARSEC fits

Se varían manualmente la metalicidad y el enrojecimiento de cada cúmulo para que su CMD se ajuste a isocronas con edades razonables (apéndice A.4). Se encuentran desviaciones remarcables entre la metalicidad de la literatura y lo aquí encontrado (Tabla 5).

In previous sections, we have found indications that the literature metallicity and/or the extinction of the clusters may not be accurate, with hints that, in general, the extinction may be underestimated. For this reason, we adjusted the metallicity and/or extinction of each cluster until we found a good visual agreement between most of the stars in the CMD and the isochrones. That is, the extinction of all stars and the metallicity of the isochrones are modified to achieve a better fit. Table 5 shows the Harris (1996) extinctions and the literature metallicities compared with the manually adjusted extinction and metallicity to obtain the best fit with isochrones of reasonable age.

GC Name	E(B-V) (HARRIS) [mag]	E(B-V) (FIT) [mag]	Metallicity (LIT) [dex]	Metallicity (FIT) [dex]
NGC_104	0.04	0.04	-0.73 ± 0.02	-0.60
NGC_5904	0.03	0.03	-1.19 ± 0.05	-1.09
NGC_6205	0.02	0.02	-1.46 ± 0.04	-1.37
NGC_6218	0.19	0.23	-1.26 ± 0.03	-1.37
NGC_6341	0.02	0.04	-2.22 ± 0.03	-2.22
NGC_6362	0.09	0.09	-1.07 ± 0.01	-0.95
NGC_6397	0.18	0.20	-2.02 ± 0.04	-1.75
NGC_6752	0.04	0.08	-1.47 ± 0.03	-1.54
NGC_6809	0.08	0.15	-1.75 ± 0.04	-1.85
NGC_7099	0.03	0.06	-2.31 ± 0.05	-2.24

Table 5: Harris (1996) extinctions and the calculated extinctions to obtain the best fit with the isochrones in the CMD. Also, the metallicity found in the literature and the best guess metallicity (to achieve a good fit with the BaSTI isochrones) are added. In bold are the values set here. Note that practically all calculated metallicities vary from the metallicities in the literature.

It is clear that extinction is underestimated in six of the ten clusters in our sample. When extinction is markedly underestimated, it is clearly appreciable that the mismatch between the cluster CMD and the isochrones is due to extinction and not metallicity because the whole CMD is shifted by the same amount with respect to the isochrones. Although the absolute differences in extinction are small, they have an important effect on the CMD. It is not excluded that there is differential extinction in some of the clusters, that is, that stars in the same cluster may have different extinctions. However, this in principle, is not to be expected since GCs are compact and not very extensive in the sky plane. In addition, we have seen that when there is a clear shift it affects all the stars in the CMD equally, thus showing a significant absence of differential extinction.

Regarding metallicity, there seems to be a slight trend to underestimate metallicity in the literature. But this is not as evident as the problem of extinction. Some adjusted metallicities are outside the error bars of literature metallicities. It should be noted that the manual fit is not as accurate as any measurement found in the literature but there is a small indication that for some clusters (such as NGC 6397) the metallicity should be checked to avoid possible systematic errors in the metallicity calculation.

Figures 14 to 17 show the best fit found for the BaSTI and PARSEC isochrones using the E(B-V) FIT in Table 5, and adjusting the metallicity independently for each library. BaSTI isochrones are able to fit to the distribution of stars in the entire CMD correctly. The best

metallicities for PARSEC are slightly lower than the best ones found for BaSTI. It is observed, especially in Figure 15 that PARSEC does not fit the beginning of the RGB as well as BaSTI. For example, if we look at the green isochrone in NGC 104, we can see how the BaSTI one correctly fits to the cluster but the PARSEC one is not able to adjust the beginning of the RGB although it correctly fits the main sequence and the turnoff. A different combination of extinction-metallicity is probably needed to fit correctly with PARSEC isochrones. All CMDs with the fitted BaSTI isochrones for all the clusters can be found in the appendix A.4.

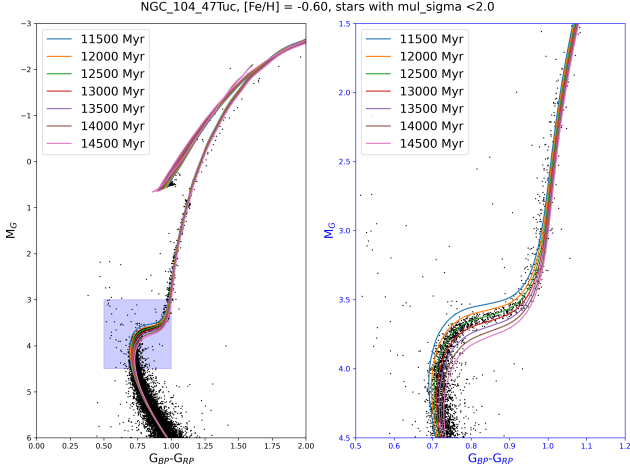


Figure 14: CMD of the extinction corrected ($E(B-V)=0.04$) star selection of NGC 104, overlapped with the manually adjusted BaSTI isochrones ($[Fe/H]=-0.60$).

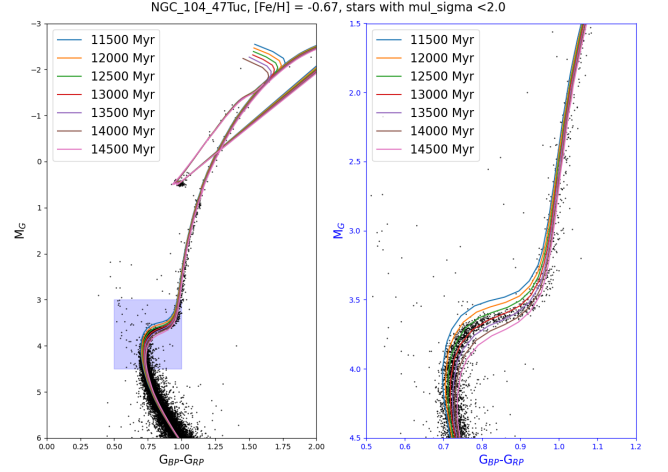


Figure 15: CMD of the extinction corrected ($E(B-V)=0.04$) star selection of NGC 104, overlapped with the manually adjusted PARSEC isochrones ($[Fe/H]=-0.67$).

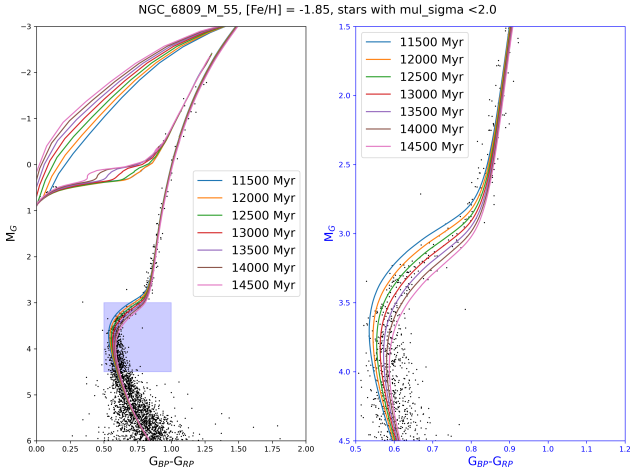


Figure 16: CMD of the extinction corrected ($E(B-V)=0.15$) star selection of NGC 6809, overlapped with the manually adjusted BaSTI isochrones ($[Fe/H]=-1.88$).

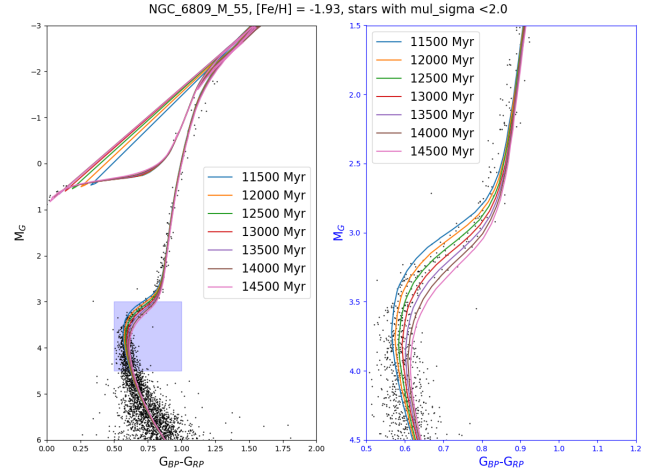


Figure 17: CMD of the extinction corrected ($E(B-V)=0.15$) star selection of NGC 6809, overlapped with the manually adjusted PARSEC isochrones ($[Fe/H]=-1.93$).

6.4. Is it possible to determine ages and metallicities of GCs with this method?

Con los métodos anteriormente mostrados es muy difícil determinar una metalicidad y edad precisa del GC. En general, hay diferentes combinaciones de metalicidad, extinción y edad que

son compatibles con el CMD de un GC dado. Por lo tanto, es necesario otro método para encontrar ajustes de isocronas si se quiere determinar la edad y metalicidad de los cúmulos, así como mejorar la exactitud de las metalicidades y extinciones de la literatura.

Attempting to determine the age and the metallicity of these GCs by this method is problematic. Inaccuracies in extinction or metallicity lead to a wide variety of combinations of extinctions and metallicities that fit the observed CMD.

As an example, Figures 18 and 19 show two different fits with the BaSTI isochrones to the CMD of NGC 104. In Figure 18 the Harris (1996) extinction is maintained and the metallicity is increased. In Figure 19 the Harris (1996) metallicity is maintained and the extinction is increased. Both settings are compatible with the CMD showing the difficulty to determine the parameters of the cluster with this method. On the other hand, even if you have a good fit you cannot determine a precise age because there are many isochrones of different ages that are compatible with the CMD.

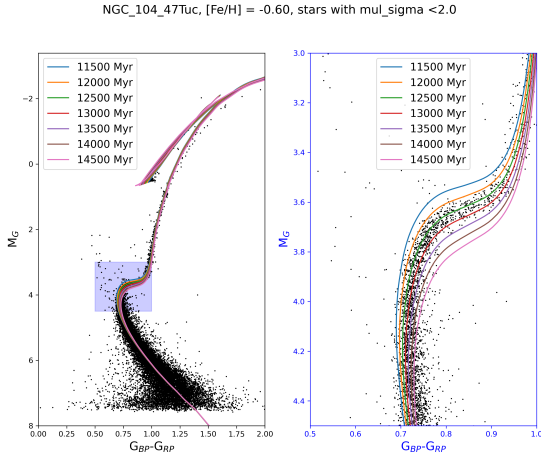


Figure 18: CMD of the extinction corrected ($E(B-V)=0.04$) star selection of NGC 104, overlapped with the manually adjusted BaSTI isochrones ($[Fe/H]=-0.60$).

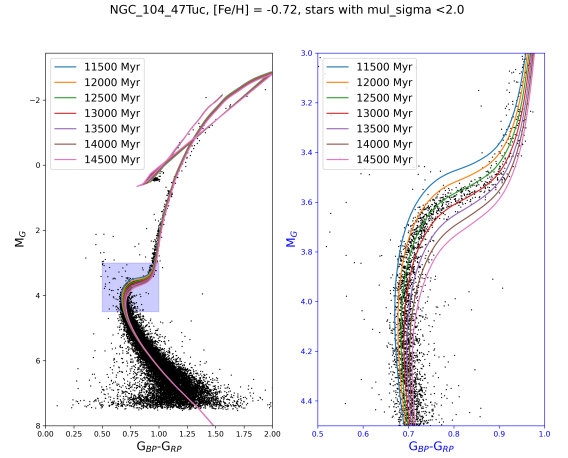


Figure 19: CMD of the extinction corrected ($E(B-V)=0.06$) star selection of NGC 104, overlapped with the manually adjusted BaSTI isochrones ($[Fe/H]=-0.72$).

6.5. Testing the SFH calculation method with synthetic clusters

Se analiza la SFH de los cúmulos sintéticos. Con estos resultados se encuentra que la exactitud del método mejora según la edad de la población es más joven, lo que concuerda con lo esperado por los modelos teóricos. En este caso no se ven dependencias importantes con el número de estrellas, concluyendo que a partir de un número razonable de estrellas las diferencias entre las SFHs calculadas son mínimas. La precisión del método aumenta según se disminuye el tamaño de los bins. Sin embargo, se ve también que hay un límite a partir del cual no es recomendable disminuir más el tamaño de los bins a partir de `recast` 1.0. Esto es porque los intervalos en color y magnitud necesarios para distinguir poblaciones con edades correspondientes a 2 bins consecutivos son comparables con los errores observacionales. Por otro lado, se analizan con estos bins los resultados del cálculo de la SFH para los cúmulos globulares sintéticos. Se encuentran muy buenos resultados en los de alta metalicidad. Para los

de baja metalicidad parece que el método no ha recuperado del todo bien los cúmulos pero es claramente debido al bajo número de estrellas que se tienen en estas metalicidades. Aún así, las diferencias entre ambas selecciones son razonables y no parece que el algoritmo esté implementando ninguna dependencia apreciable, puesto que los problemas encontrados son claramente debidos al data set de entrada. Es de destacar que el método consigue recuperar estrellas con bajas metalicidades.

6.5.1. Accuracy and precision of the SFH calculation as a function of bin size

In this section we analyze the results about the size of the age bins discussed in section 5.4.1 and how they affect the calculated SFH, as well as the precision and accuracy of the method for a dataset like the GCNS. As the synthetic clusters are simple populations with a known and narrow age and metallicity, it is appropriate to calculate the precision and accuracy of the method from these test.

First, the results of the SFH calculated for each age bin size (section 5.4.1) are shown in the following figures. We used the data from section 4.2.2 where we simulated seven synthetic clusters spaced 2 Gyr (from 0.2 Gyr to 12 Gyr). The CMDs that best fits the input data as calculated for the extreme bin sizes by CMDft.Gaia are shown in Figure 20.

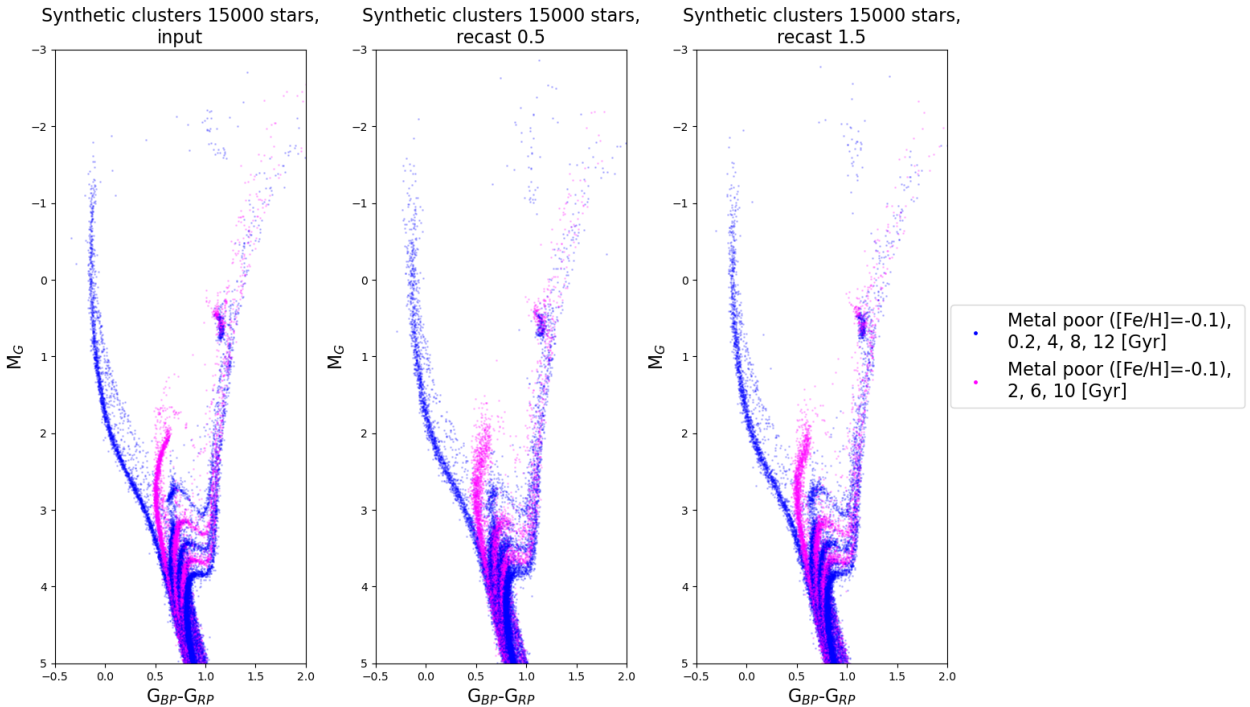


Figure 20: Left panel: CMDs of the sample of 15000 stars of synthetic clusters with 7 different ages (± 0.02 Gyr in age) and one metallicity ($[\text{Fe}/\text{H}] = -0.1 \pm 0.05$ dex in metallicity). Central and right panel: CMDs calculated with two different `recast` for the sample of 15000 stars in the input CMD. Figures including the CMD calculated for all `recast` are shown in the appendix B.4.

Clearly a CMD very consistent with input data is obtained. The recovered sequences of the synthetic clusters are tighter in `recast 1.5` compared to `recast 0.5`, with the sequences in the first more similar to those of the input CMD (though still somewhat more dispersed). To

quantitatively analyze the differences in the results with different bins sizes it is necessary to analyze the SFH in the age-metallicity plane.

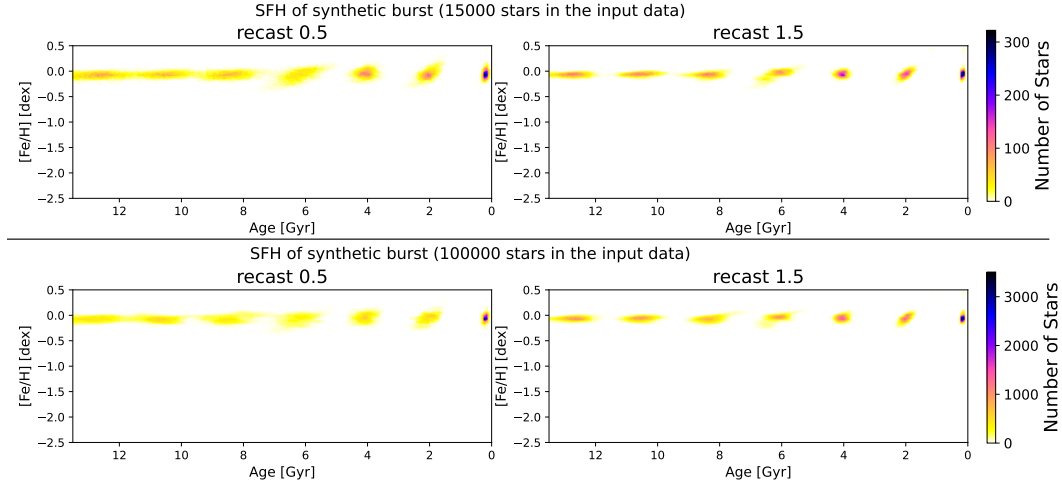


Figure 21: SFH in the age-metallicity plane of synthetic clusters of 15000 stars and 100000 stars for 2 age bins (recast 0.5 and recast 1.5).

In Figure 21, the recovered SFH, in the form of age-metallicity relation, for the most extreme recast and the 15000 star sample are shown. However, in appendix B.4 we display those of all the recast. It can be seen that, as the size of the age bins gets smaller (higher recast) the recovered synthetic clusters are better defined, being less wide in age and metallicity. This is more clearly seen in Figure 22 where we display the histograms of the number of stars as a function of age. In red we show the histograms of the input data and in blue we display the histograms of the calculated SFH. The most extreme recast for the two samples (15000 and 100000 stars) are shown.

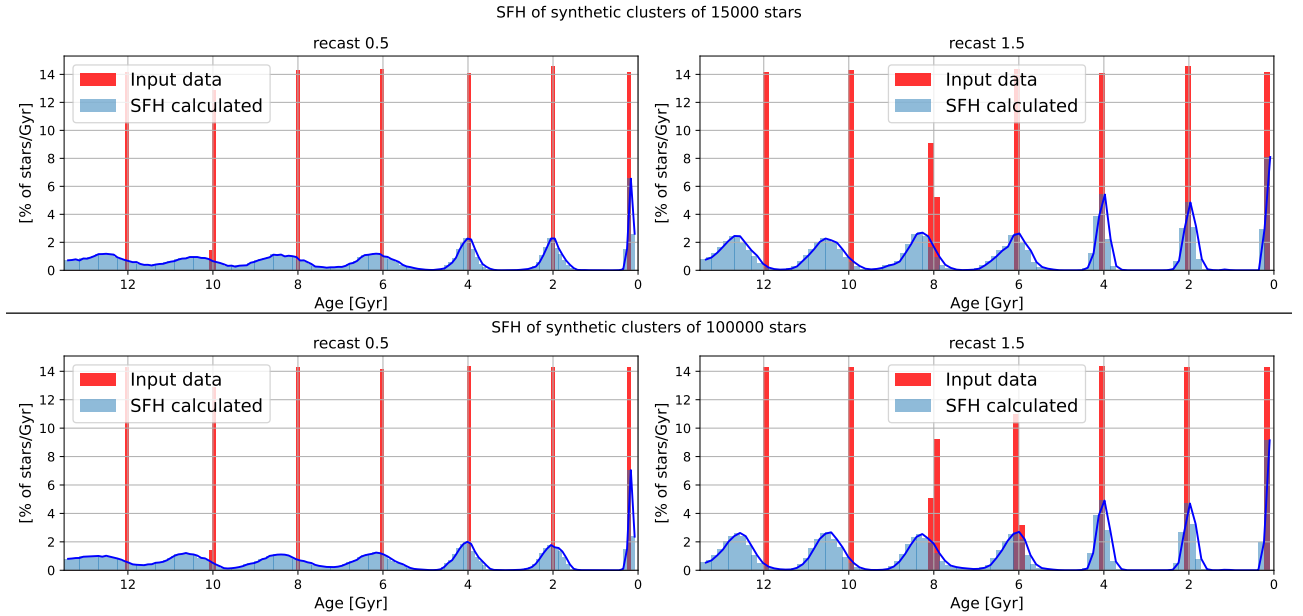


Figure 22: Percentage of stars for each age for 2 age bins size (recast 0.5 and recast 1.5) of the synthetic clusters compared with the age histogram of the input stars.

There is a clear dependence of the age resolution on the age of the synthetic cluster itself. The synthetic cluster at 0.2 Gyr is very well recuperated with little amplitude in age. As the

age of the synthetic clusters increases, age resolution is worse. This can be expected, as the size of the bins is larger at larger ages, reflecting the smaller expected age resolution due to the lower separation of the isochrones in the CMD at older ages (see Figure 20). It can also be seen that, as age increases, there is larger mismatch between the maximum of the histogram of the calculated SFH for each cluster and age of the input stars, with recovered populations being systematically older. Finally, note there are no major differences in resolution between the samples with different numbers of stars in the input data. Therefore the number of stars does not seem to be an important factor in increasing the accuracy of the method.

The accuracy and precision in the derived SFHs are discussed below in a quantitative way. The recovered age and metallicity distribution for each synthetic cluster is automatically fitted with a Gaussian in the age-metallicity plane. From the center of the Gaussian compared with the input age and metallicity it is possible to determine the accuracy in the age and metallicity determination. In appendix B.5 (Table 6) numeric values are shown for the derived accuracy and precision. The precision can be estimated from the Gaussian sigmas.

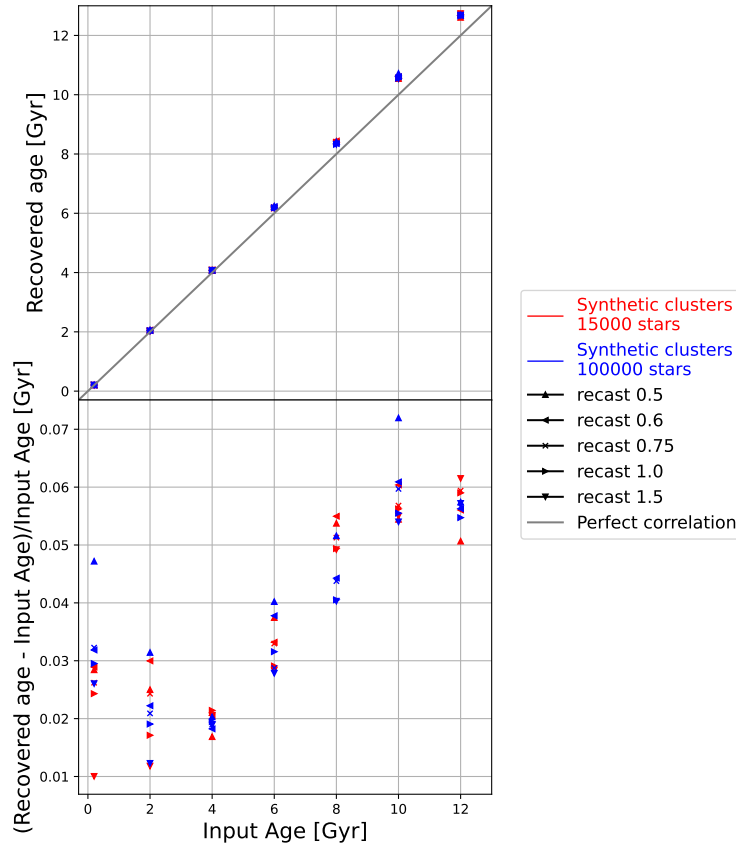


Figure 23: Upper panel: Age center calculated for each synthetic cluster from the SFH solution (recovered age) versus the age of the clusters in the data input (input age). Results for different age bins sizes and different number of stars in the synthetic clusters are shown, as indicated by different symbols described in the labels on the right Bottom panel: relative error in the age calculation of each synthetic cluster versus their input age.

Figure 23 shows (top panel) the recovered age of the SFH with respect to the age of each synthetic cluster (input age) for all the different **recast**. The relative errors of the recovered ages are included in the bottom panel. There is an entirely expected trend to be more accurate at young ages as explained above (even reaching 3 times better accuracy at 2-4 Gyr compared to 10-12 Gyr). There does not seem to be a significant dependence of the accuracy on age bins size or with the different number of stars. In all cases, age is overestimated. At very young age there is an important dispersion between the different **recast**, with smaller bin size providing

a significantly better age accuracy at ages $\lesssim 2$ Gyr.

The precision of the method is calculated from the sigma of the Gaussian fitted on the age axis (or from the projection on the age axis if the Gaussian is not aligned with the axes). Figure 24 displays a measure of the age precision (defined as two times the age sigma of the fitted Gaussian) for each synthetic cluster solution as a function of the five bins sizes corresponding to the five recast.

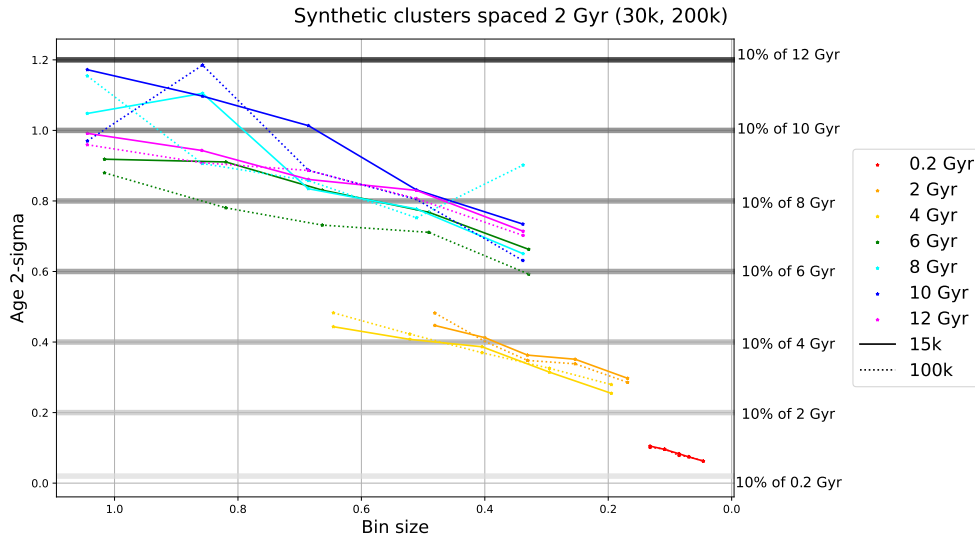


Figure 24: 2 times age sigma of the fitted Gaussian (for each synthetic cluster) versus the age bin size at the center of each synthetic cluster solution. Each point corresponds to a different **recast** (0.5 to 1.5 from left to right) and each color of the lines corresponds to a different synthetic cluster. The solid lines are the solutions of the sample of 15000 stars and the dashed lines are the solutions of the sample of 100000 stars.

The figure shows that the recovered age sigma is smaller, by almost a factor of two, for the smallest bins compared with the larger bins, and thus the age precision gets better as bin size decreases.

Figure 24 also shows that the precision will not only depend on the size of the bin, but on the age of the recovered population as well. Comparing the 6 to 12 Gyr clusters with the 2-4 Gyr clusters for the same age bin size (0.3-0.6 Gyr) show that the sigma of 6-12 Gyr clusters is 0.6-0.8 Gyr while the sigma for the 2-4 Gyr clusters is about 0.5. **Recast** higher than **recast** 0.75, corresponding to the two points with the smaller bins size in each sequence, are able to recover some of the clusters (12 Gyr, 10 Gyr, 8 Gyr, 4 Gyr) with an age precision of at least 10 % of the cluster age. The 0.2 Gyr, 2 Gyr and 6 Gyr clusters are recovered with a precision slightly lower than 10 % of the cluster age. A slight dependence of the precision on the number of stars in the synthetic clusters is noticeable. The precision improves (the sigma of the recovered cluster decreases) as the number of stars increases. This seems to be more remarkable at higher **recast**.

In general the **recast** 0.5 and 0.6 (the first two point from the left in all the synthetic clusters in the Figure 24) are not very suitable because of the obvious loss of resolution. In view of these figures it appears that **recast** 1.5 (last point) is the best option and one could expect that testing with even smaller age bins would improve the precision of the method. However, one must take into account the ability to differentiate populations with such small age differences with the theoretical models, specially at intermediate to old ages, where the isochrones of different ages are very close together. For example, the difference in (color, magnitude) of the turnoff point of solar metallicity isochrones 1 Gyr apart at 4 Gyr and at 10 Gyr is (0.03, 0.4), (0.01, 0.09) respectively. One criteria to decide whether a given set of age

bins is adequate could be to compare the color and magnitude differences of the turnoff point of the isochrones defining each age bin with the typical color and magnitude errors of the stars located around the turnoff position of the same isochrones.

Figure 25 displays (black points joined by a dot-dashed line) the difference in magnitude/color of the turnoff between the extremes of the age bin as a function of the mean age of the bin, for the five recast. To obtain this information we used isochrones from the BaSTI library and derived the magnitude/color of the turnoff for the ages of the extremes of each bin. In general, it was necessary to interpolate the magnitude/color since the libraries offer the turnoff points in the CMD for isochrones with ages that are not exactly the ones required here.

The solid colored lines in Figure 25 represent the typical (mean) error in magnitude (due to both photometric errors and distance errors) or color (due solely to photometric errors) for stars in the GCNS within the range of color and magnitude defined by the turnoff point of the isochrones at the extremes of the corresponding bin. The dotted lines indicate the mean error $\pm 1 \sigma$. It can be seen that the typical magnitude/color errors of the stars in the CMD around the turnoff point are smaller than the magnitude/color separation of the extremes of the corresponding bins, in the whole age range for all recast. However, for **recast 1.5**, at many ages the minimum interval in magnitude is comparable with the observational errors ($< 1\sigma$). In **recast 1.0** the mean errors are at least 1σ away from the magnitude intervals. Regarding the comparison of the size of the color intervals with the mean photometric errors ($\pm 1 \sigma$), for **recast 0.75** and **1.0**, they are consistent, while for **recast 1.5**, the mean errors $\pm 1\sigma$ are clearly larger than the color intervals.

Considering that, as discussed earlier, **recast 0.5** and **recast 0.6** clearly degrade the age resolution, we conclude that **recast 1.0** and **recast 0.75** could be a good choice (the later likely being somewhat conservative).

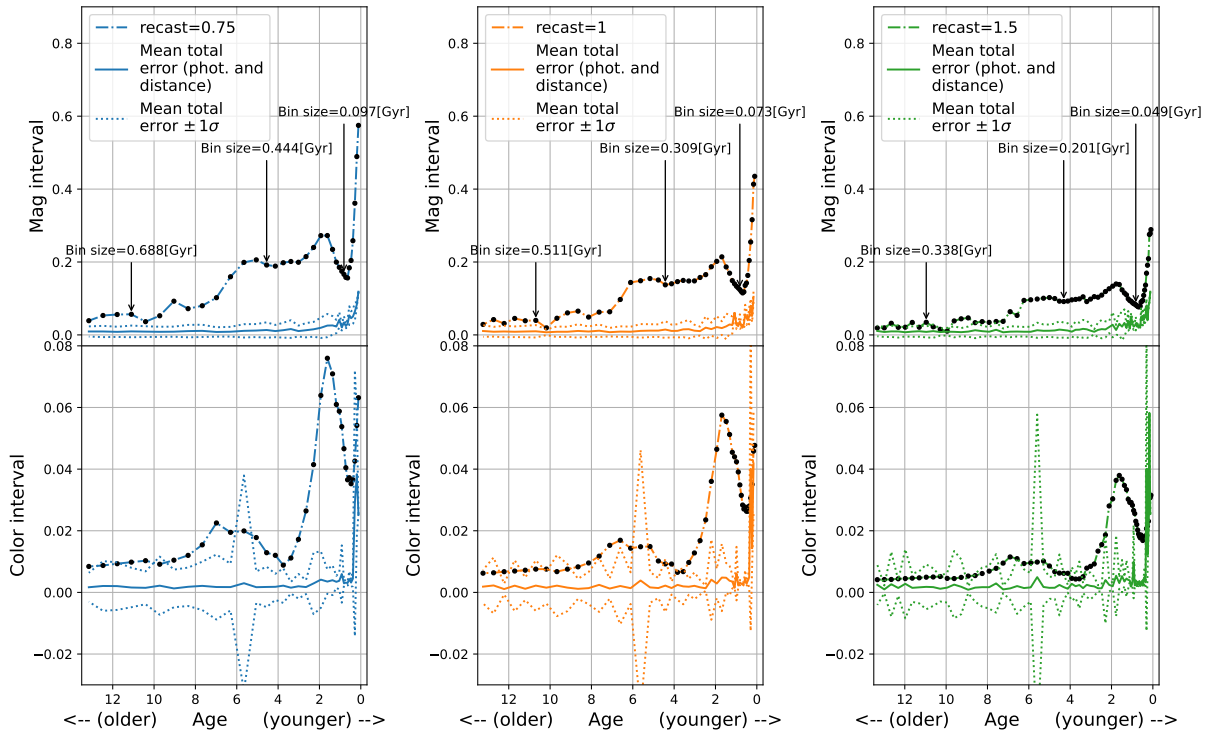


Figure 25: Black dots and dot-dashed lines: difference in magnitude (top) and color (bottom) in the turnoff between the extremes of the bins versus the average age of the bin for **recast 0.75**, **1.0** and **1.5**. Colored solid lines: mean observational errors (both photometric and distance errors, in case of magnitude) of stars in the GCNS in turnoff CMD zone. As a guide some age bins sizes are shown.

6.5.2. Testing the SFH calculation method for synthetic GCs

As a further test of the correct performance of the method, the SFHs of the synthetic GCs described in section 4.2.1 are calculated.

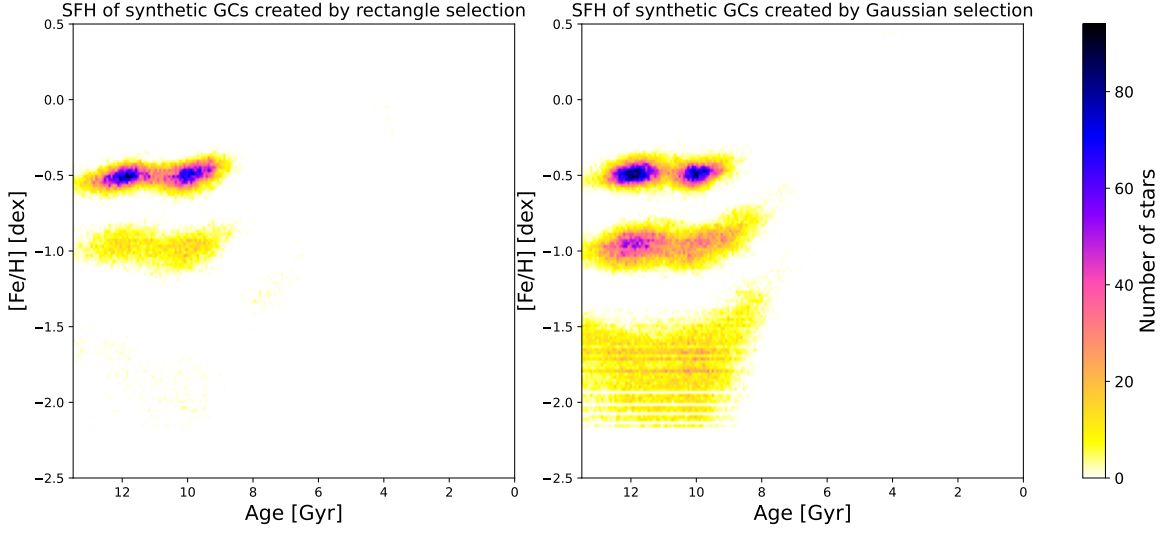


Figure 26: SFH in the age-metallicity plane of synthetic globular clusters created in section 4.2.1, both with rectangle selection and Gaussian selection.

In Figure 26 it can be seen that the most metal poor clusters are recovered in a diffuse way. In the rectangular selection the most likely explanation is the small number of stars. It should be remembered that the input CMD had less than 200 stars per metal poor cluster. This problem can be solved by increasing the number of stars in the mother diagram, so it is not a question of the method but of the input data. In the Gaussian selection, some metal poor population is recovered but it is not as accurate and precise as expected. However, it should be remembered that the Gaussian selection was biased at low metallicities due to the few stars in the mother diagram. In fact, if compared to the input data (Figure 4) the SFH has a similar profile with more stars with slightly higher metallicities than requested in the selection. The intermediate and high metallicity synthetic GCs are much successfully recovered, specially in the case of the Gaussian selection which created more populated samples. In this case, the two clusters at different ages are clearly noticeable.

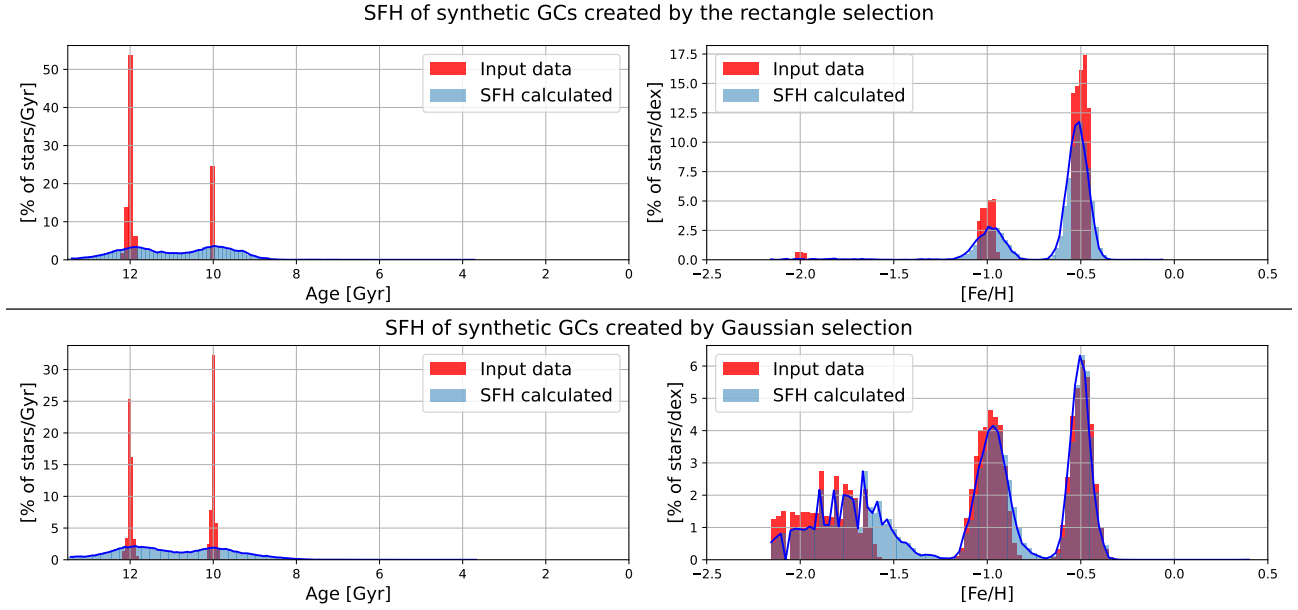


Figure 27: Left panels: Histogram of the number of stars as a function of age for each selection (rectangle and Gaussian) from the same data set (section 4.2.1). Right panels: Histogram of the number of stars as a function of metallicity for each selection. Input data is in red, and recovered age and metallicity distributions are in blue. All the data in this figure has been normalized to the total number of stars in the input or recovered data for a better comparison.

Figure 27 allows a more quantitative comparison between the distributions in age and metallicity of the stars in the input synthetic GCs, and in the recovered GCs. In spite of the lower number of stars in the rectangular selection, the results are quite similar in both cases: the peak of the recovered age is in good agreement with the input age, even though the age distributions are quite wide. When populations are as thin in metallicity as in the rectangular selection, they are recovered with a larger width in metallicity than in the input data (as was the case with the age). However, if the populations are sufficiently large in the metallicity range as in the case of Gaussian selection, the distribution of the input data is recovered very well in metallicity.

7. Conclusions and future work

7.1. Observational data quality

En este trabajo se ha observado una gran calidad en los datos proporcionados por *Gaia*. Además, se han comparado los errores observacionales del mejor data set que proporciona *Gaia* (GCNS) con la precisión de los modelos teóricos. En los cúmulos globulares, es posible limpiar los CMDs de estrellas externas al cúmulo sin dificultad. En cuanto a los datos adicionales de los cúmulos globulares se ha visto que es necesaria una mejora en las medidas de extinción y metalicidad para poder ajustar isocronas correctamente.

Throughout this work we have seen remarkable quality of the data provided by *Gaia* EDR3, both in the analysis of GCs and of the GCNS when comparing observational errors with the smallest bin sizes used for the SFH derivation (see Figure 25). It is also worth noting the impressive work done by Vasiliev & Baumgardt (2021) in calculating a probability of membership for each star from which very good results are obtained, thanks to the excellent *Gaia* data quality. With the help of this membership probability and the elimination of stars affected by crowding it has been possible to clean the CMD for each cluster satisfactorily. In addition, it is concluded that the measurements of GCs extinction and metallicity must be more accurate in order to make a good match with theoretical models. The Harris (1996) catalogue is still useful as a guide reference but for works such as that done here, better measurements are needed. Above all, a more accurate extinction is required, which has the most effect when fitting the isochrones.

7.2. On the comparison between GC CMDs and isochrones. Differences between BaSTI and PARSEC

Se han observado diferencias entre los datos observacionales y los modelos teóricos. Siendo quizás la zona de la RGB la región con mayor margen de mejora en los modelos, sin embargo solo se han encontrado pequeñas desviaciones en algunos casos. Se han encontrado diferencias sistemáticas entre las librerías de PARSEC y BaSTI: las isocronas de PARSEC son más rojas que las de BaSTI en la secuencia principal y en el turnoff. Esto puede tener implicaciones en los resultados de la historia de formación estelar que van a merecer análisis en el futuro.

We have analyzed the behavior of the stellar evolution models through comparison with the observed CMD of GCs.

- With the method used here it is not possible to determine with precision the age or metallicity of GCs as there are degeneracies between metallicity, extinction, distance and age. An statistical method that would allow to find a best fit by searching in the metallicity, extinction, distance and age spaces within the errorbars of all these parameters should be considered.

- BaSTI and PARSEC isochrones differ from each other at least at old ages. PARSEC isochrones are redder than those of BaSTI in the turnoff region and in the main sequence. This difference increases as the metallicity of the isochrones increases. This is expected to have an impact on the calculation of the SFH. Slight deviations between the sequences in the GCs and the isochrones have been seen in the RGB, which may indicate a possible room for improvement of the models in this area of the CMD. It should not be forgotten that the RGB corresponds to a very advanced stellar evolutionary phase, so the presence of errors is greater.
- It is proposed as future work to test the SFH calculation method with the two stellar evolution libraries. This would allow to explore the possible dependencies of the SFH results with the stellar evolution models.

7.3. Performance of the SFH calculation method

En este trabajo se ha analizado la precisión y exactitud del método de cálculo de la SFH. Se han encontrado fuertes dependencias, tanto en la precisión como en la exactitud, con la edad de los datos de entrada, así como, con el tamaño en edad de las poblaciones simples creadas por el método (bins de edad). Se encuentra una mejor resolución y precisión a edades jóvenes así como una ligera dependencia de la precisión con el número de estrellas de los datos de entrada. Además, se ve que una buena opción para datos con errores similares a GCNS es un tamaño de bin de edad correspondiente al `recast` 1.0 y 0.75. Se propone seguir la misma metodología que la realizada en este trabajo pero con los tamaños de los bins de metalicidad, además de analizar los tamaños de los bins adecuados para otros data sets.

The accuracy and precision of the SFH calculation method has been analyzed. In particular, the dependencies of precision and accuracy on i) the size of the age bins, ii) the age of the input population and iii) the size (number of stars) of the input population have been analyzed:

- With respect to the accuracy, it is concluded that it depends on the size of the age bins used. The smaller the bin the better the accuracy of the method. Another important dependence of the accuracy is with the age of the populations being analyzed. The smaller the age, the better the accuracy. It should be noted that the age is always overestimated, around 2 % in young age populations and around 5 % in old age populations. No strong dependence of accuracy with the number of stars has been found.
- The precision also depends on the size of the age bins used and on the age of the populations analyzed. It has been found that the method is very precise in determining the age at young ages (populations are recovered with an age width around 0.1-0.4 Gyr) and less precise at old ages (populations are recovered with an age width around 0.9 Gyr), which is in agreement with what is expected from stellar theoretical models. A small improvement in precision can be observed if the number of stars in the input data is increased.

Defining the size of the age bins is an essential problem in the SFH calculation, and a good choice is very important to obtain reliable results. Different sizes of age bins have been analyzed

in depth, concluding that `recast` 1.0 is the best option along with `recast` 0.75, being this somewhat conservative. In this work these analyses have been performed taking into account that the input data set is GCNS. However, in future works with other data sets the same methodology as here can be followed to correctly choose an appropriate age bins size. A future proposal is to perform the same type of analysis presented here but for the metallicity bins size. Something more difficult to do in the future but feasible is to calculate the SFH of the GCs shown here after cleaning the CMDs. This would require simulating the observational errors of these clusters (which are significantly larger than in GCNS) in the mother diagram. But this would allow to calculate the ages and metallicities of these clusters with probably very accurate results.

8. Acknowledge

This work has made use of data from the European Space Agency (ESA) mission *Gaia* (<https://www.cosmos.esa.int/gaia>), processed by the *Gaia* Data Processing and Analysis Consortium (DPAC, <https://www.cosmos.esa.int/web/gaia/dpac/consortium>). Funding for the DPAC has been provided by national institutions, in particular the institutions participating in the *Gaia* Multilateral Agreement. This research has made use of the NASA/IPAC Extragalactic Database (NED), which is operated by the Jet Propulsion Laboratory, California Institute of Technology, under contract with the National Aeronautics and Space Administration. The numpy ([Harris et al., 2020](#)), matplotlib ([Hunter, 2007](#)) and vaex python packages have been used intensively in this work.

9. Code availability

The reader is offered a software that searches for GCs in the [Harris \(1996\)](#) according to extinction, distance and metallicity. For the clusters found, the methodology used here is applied to filter their stars and fit the isochrones. Therefore, any GC CMD can be obtained (among other diagrams) and the isochrone fitting based on the methodology of this TFG is performed. For more details read the README on the software repository. The repository is located at https://github.com/DavidMirabal/CMD_CREATOR

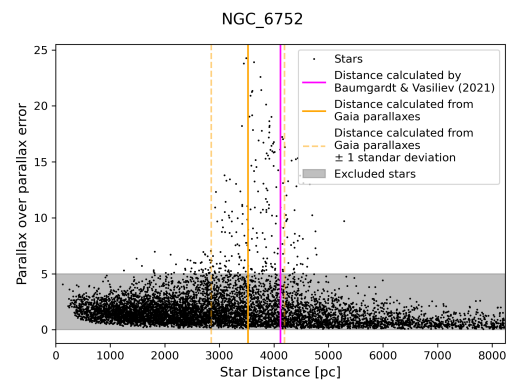
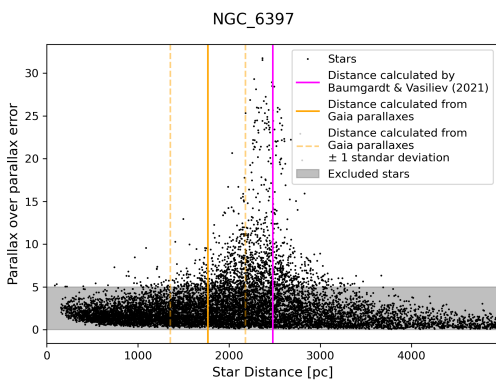
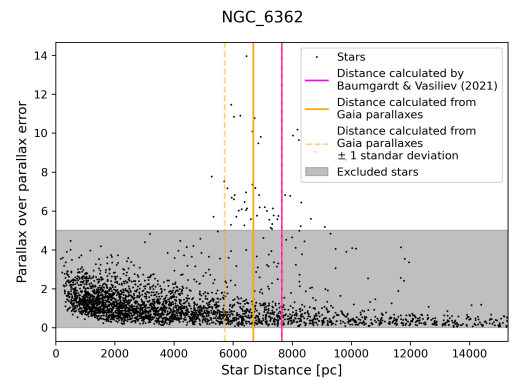
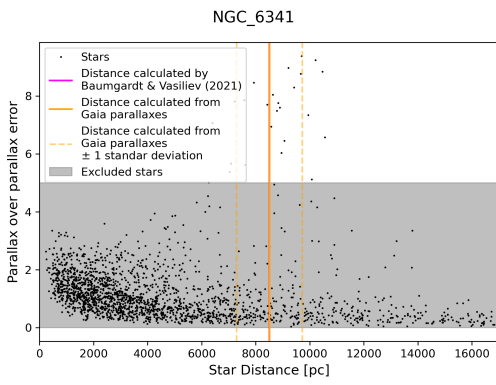
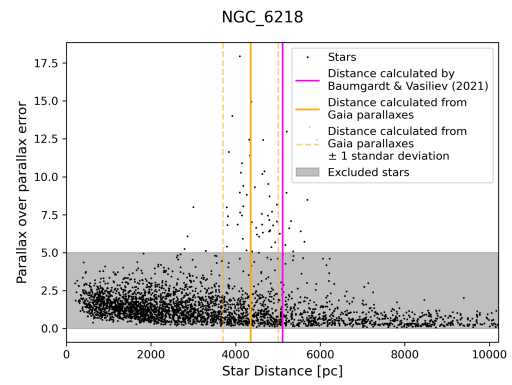
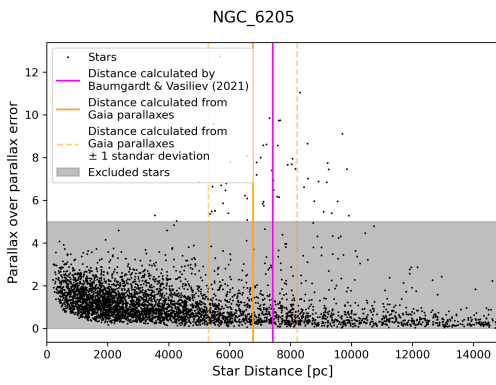
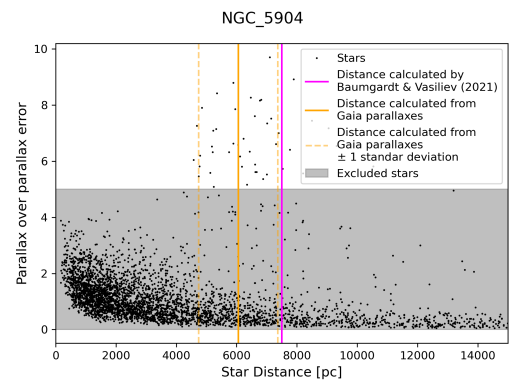
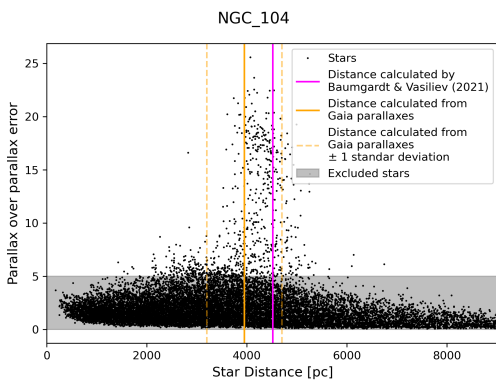
References

- Andrae, R., Fouesneau, M., Creevey, O., et al. 2018, *Astronomy & Astrophysics*, 616, A8, doi: [10.1051/0004-6361/201732516](https://doi.org/10.1051/0004-6361/201732516)
- Aparicio, A., & Gallart, C. 2004, *The Astronomical Journal*, 128, 1465, doi: [10.1086/382836](https://doi.org/10.1086/382836)
- Aparicio, A., & Hidalgo, S. L. 2009, *The Astronomical Journal*, 138, 558, doi: [10.1088/0004-6256/138/2/558](https://doi.org/10.1088/0004-6256/138/2/558)
- Barmby, P., & Huchra, J. P. 2001, *The Astronomical Journal*, 122, 2458, doi: [10.1086/323457](https://doi.org/10.1086/323457)
- Baumgardt, H., & Vasiliev, E. 2021, *Monthly Notices of the Royal Astronomical Society*, 505, 5957, doi: [10.1093/mnras/stab1474](https://doi.org/10.1093/mnras/stab1474)
- Bressan, A., Marigo, P., Girardi, L., et al. 2012, *Monthly Notices of the Royal Astronomical Society*, 427, 127, doi: [10.1111/j.1365-2966.2012.21948.x](https://doi.org/10.1111/j.1365-2966.2012.21948.x)
- Chiosi, C., Bertelli, G., & Bressan, A. 1992, *Annual Review of Astronomy and Astrophysics*, 30, 235, doi: [10.1146/annurev.aa.30.090192.001315](https://doi.org/10.1146/annurev.aa.30.090192.001315)
- Fabricius, C., Luri, X., Arenou, F., et al. 2021, *Astronomy & Astrophysics*, 649, A5, doi: [10.1051/0004-6361/202039834](https://doi.org/10.1051/0004-6361/202039834)
- Gaia Collaboration, Babusiaux, C., van Leeuwen, F., et al. 2018, *Astronomy & Astrophysics*, 616, A10, doi: [10.1051/0004-6361/201832843](https://doi.org/10.1051/0004-6361/201832843)
- Gaia Collaboration, Smart, R. L., Sarro, L. M., et al. 2021a, *Astronomy & Astrophysics*, 649, A6, doi: [10.1051/0004-6361/202039498](https://doi.org/10.1051/0004-6361/202039498)

- Gaia Collaboration, Brown, A. G. A., Vallenari, A., et al. 2021b, *Astronomy & Astrophysics*, 649, A1, doi: [10.1051/0004-6361/202039657](https://doi.org/10.1051/0004-6361/202039657)
- Gallart, C., Bernard, E. J., Brook, C. B., et al. 2019, *Nature Astronomy*, 3, 932, doi: [10.1038/s41550-019-0829-5](https://doi.org/10.1038/s41550-019-0829-5)
- Harris, C. R., Millman, K. J., van der Walt, S. J., et al. 2020, *Nature*, 585, 357, doi: [10.1038/s41586-020-2649-2](https://doi.org/10.1038/s41586-020-2649-2)
- Harris, W. E. 1996, *The Astronomical Journal*, 112, 1487, doi: [10.1086/118116](https://doi.org/10.1086/118116)
- Hidalgo, S. L., Pietrinferni, A., Cassisi, S., et al. 2018, *The Astrophysical Journal*, 856, 125, doi: [10.3847/1538-4357/aab158](https://doi.org/10.3847/1538-4357/aab158)
- Horta, D., Schiavon, R. P., Mackereth, J. T., et al. 2020, *Monthly Notices of the Royal Astronomical Society*, 493, 3363, doi: [10.1093/mnras/staa478](https://doi.org/10.1093/mnras/staa478)
- Hunter, J. D. 2007, *Computing in Science & Engineering*, 9, 90, doi: [10.1109/MCSE.2007.55](https://doi.org/10.1109/MCSE.2007.55)
- Karttunen, H., Kröger, P., Oja, H., Poutanen, M., & Donner, K. J. 2017, *Fundamental astronomy* (Springer-Verlag Berlin Heidelberg)
- Lindegren, L., Bastian, U., Biermann, M., et al. 2021, *Astronomy & Astrophysics*, 649, A4, doi: [10.1051/0004-6361/202039653](https://doi.org/10.1051/0004-6361/202039653)
- Massari, D., Mucciarelli, A., Dalessandro, E., et al. 2017, *Monthly Notices of the Royal Astronomical Society*, 468, 1249, doi: [10.1093/mnras/stx549](https://doi.org/10.1093/mnras/stx549)
- Mucciarelli, A., & Bonifacio, P. 2020, *Astronomy & Astrophysics*, 640, A87, doi: [10.1051/0004-6361/202037703](https://doi.org/10.1051/0004-6361/202037703)
- Pedregosa, F., Varoquaux, G., Gramfort, A., et al. 2011, *Journal of Machine Learning Research*, 12, 2825
- Piotto, G., Milone, A. P., Anderson, J., et al. 2012, *The Astrophysical Journal*, 760, 39, doi: [10.1088/0004-637X/760/1/39](https://doi.org/10.1088/0004-637X/760/1/39)
- Rivero, A., Gallart, C., & Monelli, M. 2022, *The accuracy of stellar evolution models to interpret Gaia photometric data: impact on the derived star formation histories (TFG)*, Universidad de La Laguna, Grado en Física
- Ruiz-Lara, T., Gallart, C., Bernard, E. J., & Cassisi, S. 2020, *Nature Astronomy*, 4, 965, doi: [10.1038/s41550-020-1097-0](https://doi.org/10.1038/s41550-020-1097-0)
- Ruiz-Lara, T., Helmi, A., Gallart, C., Surot, F., & Cassisi, S. 2022, *Astronomy & Astrophysics*, 668, L10, doi: [10.1051/0004-6361/202244127](https://doi.org/10.1051/0004-6361/202244127)
- Sakari, C. M., Shetrone, M., Venn, K., McWilliam, A., & Dotter, A. 2013, *Monthly Notices of the Royal Astronomical Society*, 434, 358, doi: [10.1093/mnras/stt1026](https://doi.org/10.1093/mnras/stt1026)
- Taylor, J. R., & Thompson, W. 1982, *An introduction to error analysis: the study of uncertainties in physical measurements*, Vol. 2 (Springer)
- Torres, J. S., Gallart, C., & Ruiz-Lara, T. 2022, *A first robust star formation history of the solar neighbourhood within 100 pc using the Gaia Catalogue of Nearby Stars (TFM)*, Universidad de La Laguna, Máster en Astrofísica
- Vasiliev, E., & Baumgardt, H. 2021, *Monthly Notices of the Royal Astronomical Society*, 505, 5978, doi: [10.1093/mnras/stab1475](https://doi.org/10.1093/mnras/stab1475)

A. Appendix: Real globular clusters

A.1. Distances to clusters



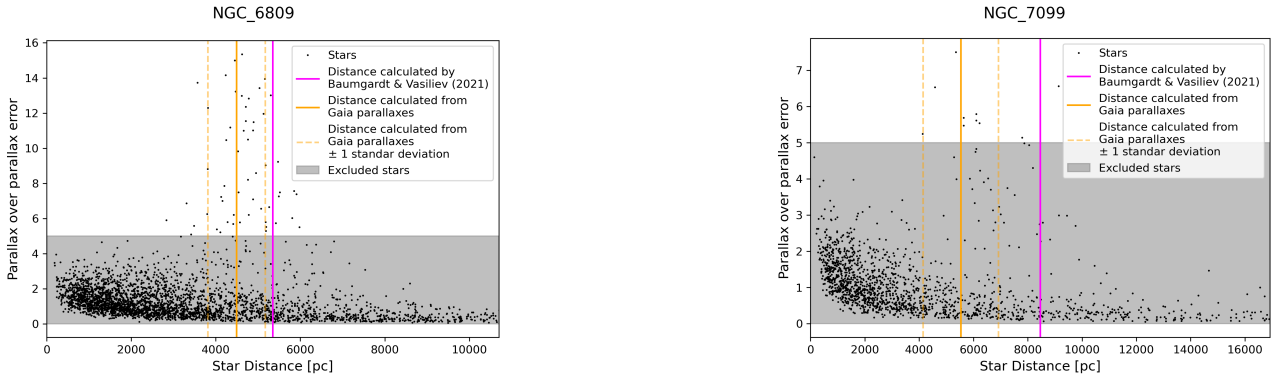
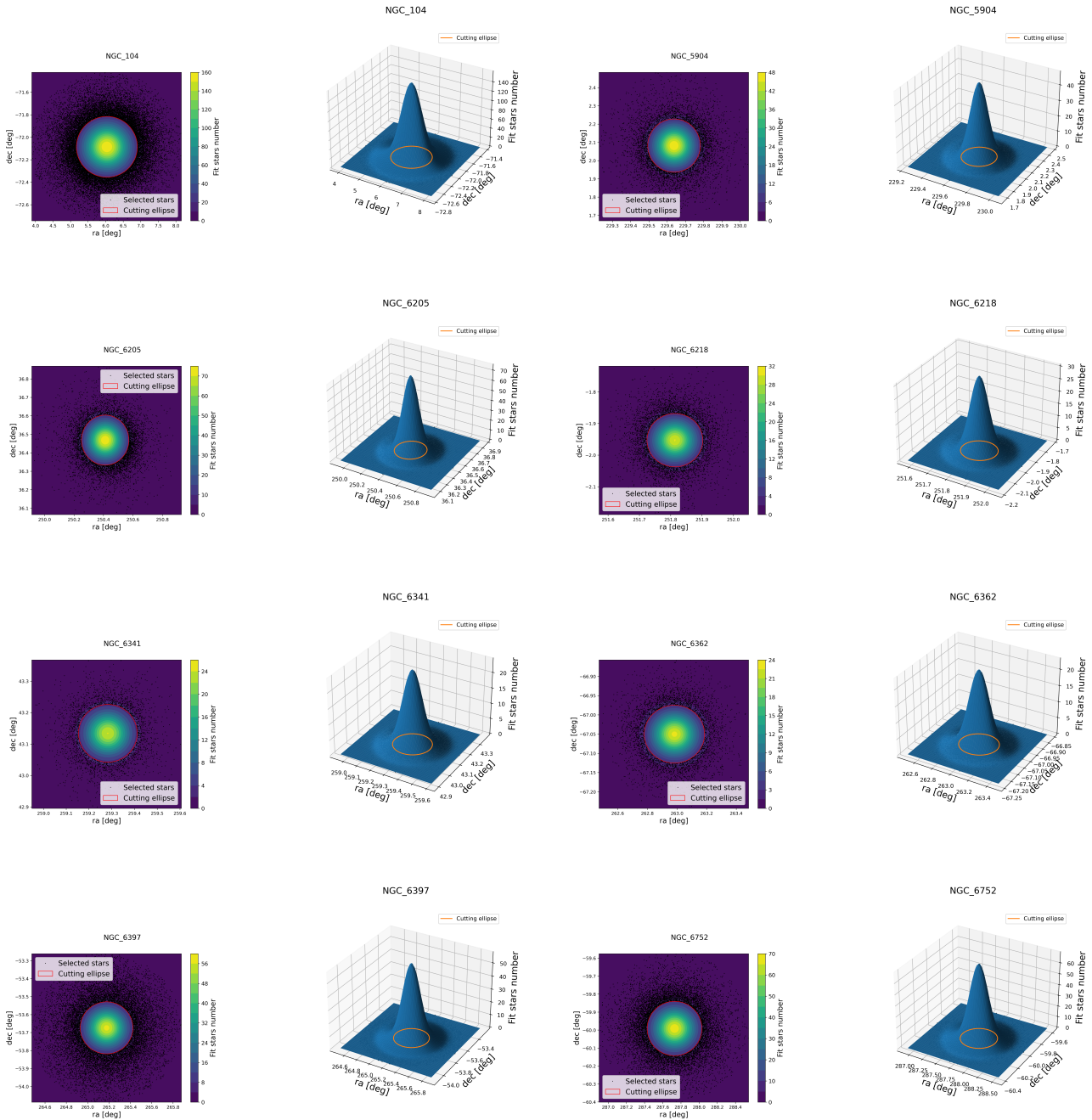


Figure 28: Parallax over parallax error versus star distance to the sun. Magenta line represents the distance calculated by Baumgardt & Vasiliev (2021).

A.2. Cluster Members selection



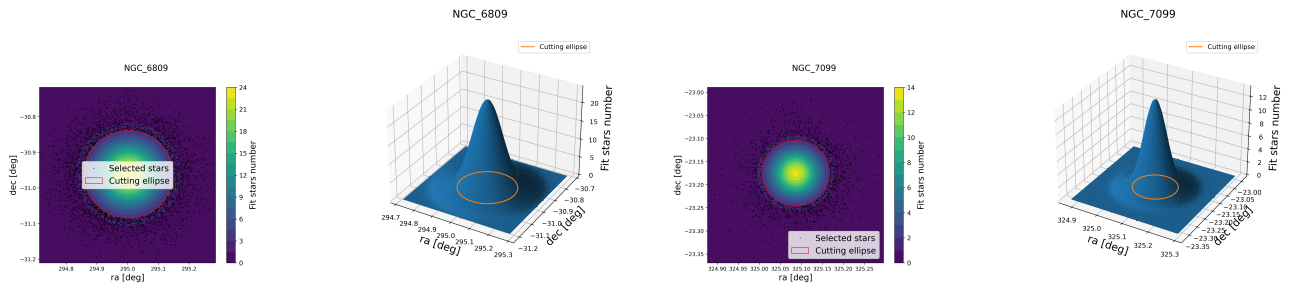
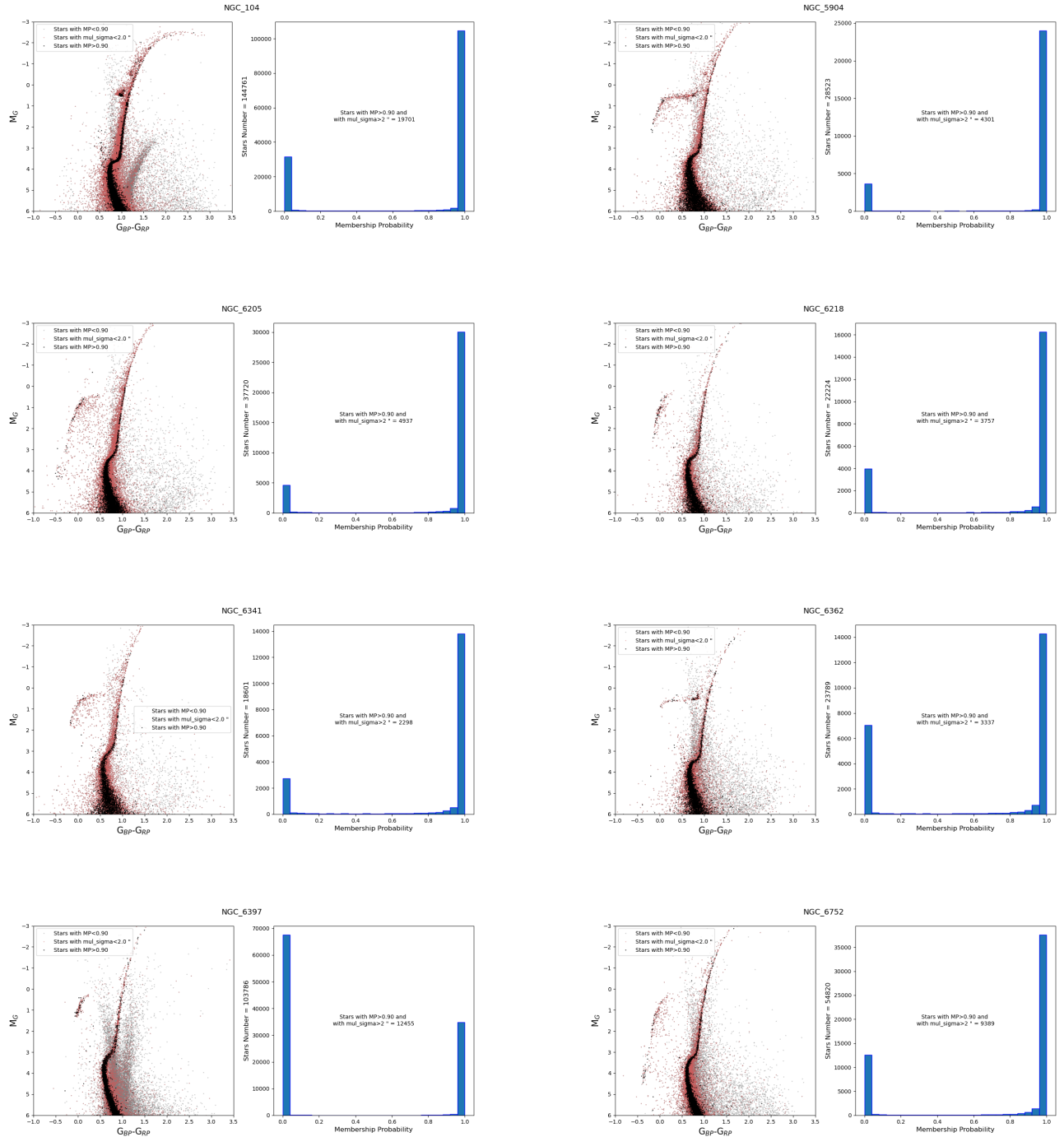


Figure 29: Stars distribution in the sky plane with the fitted Gaussian overlaid and the cutting ellipse created using `mul_sigma` and the fitted sigmas of all clusters. Also a 3D representation is shown.



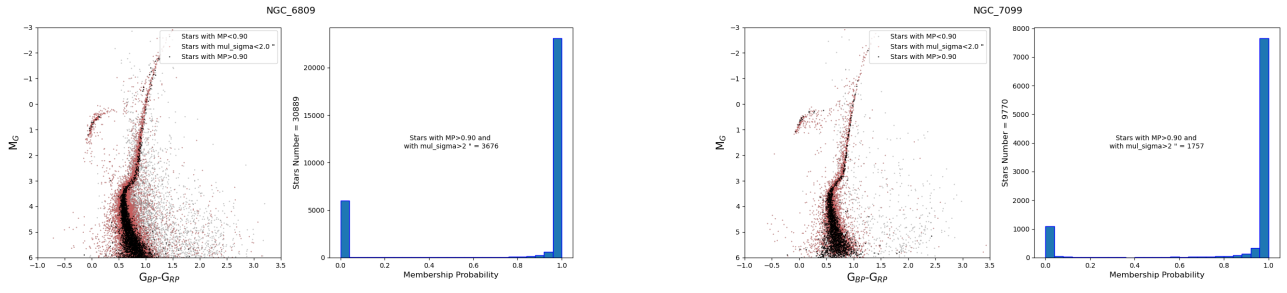
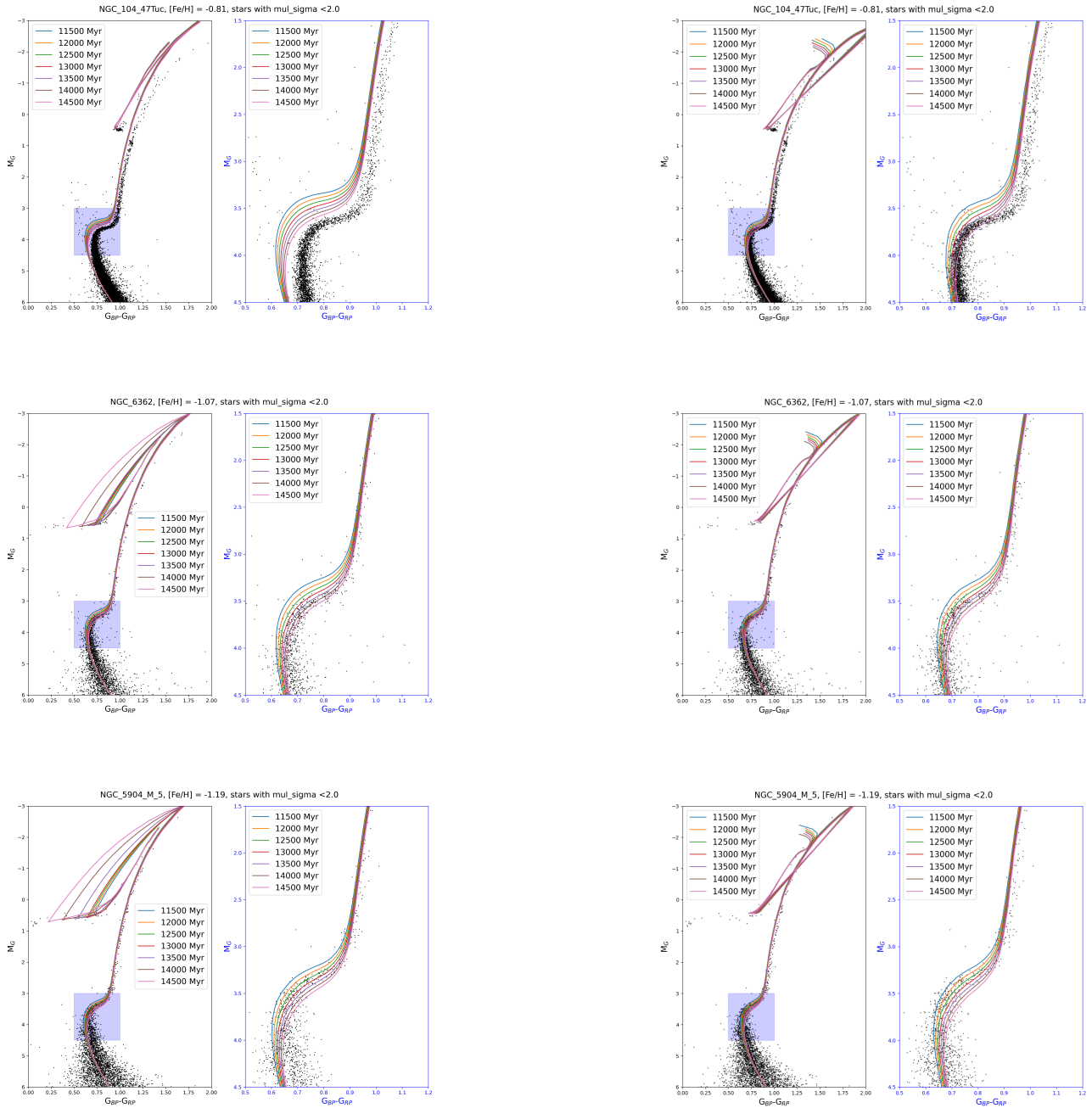
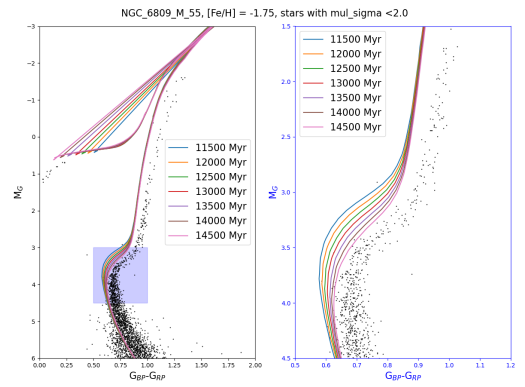
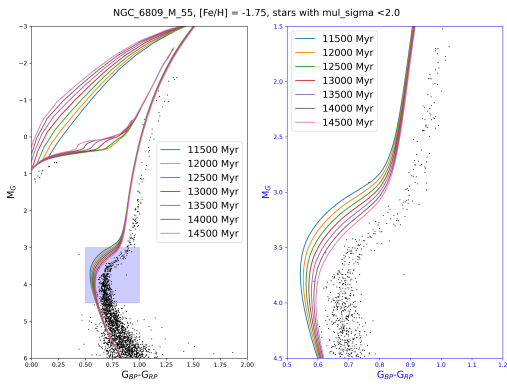
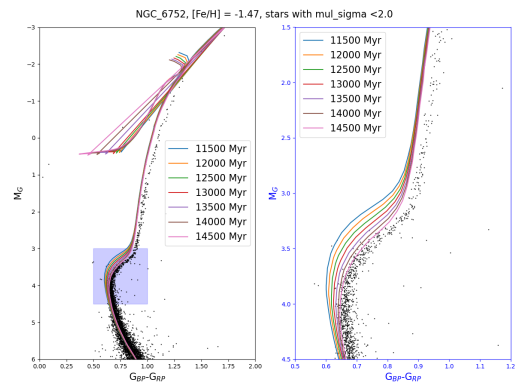
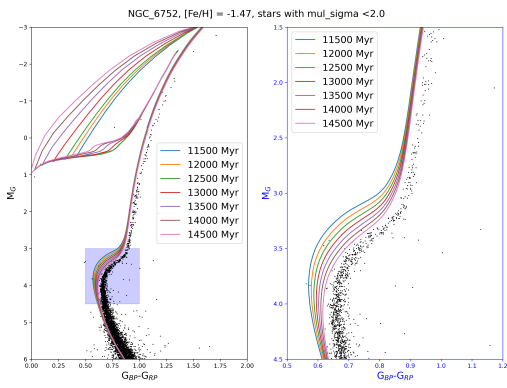
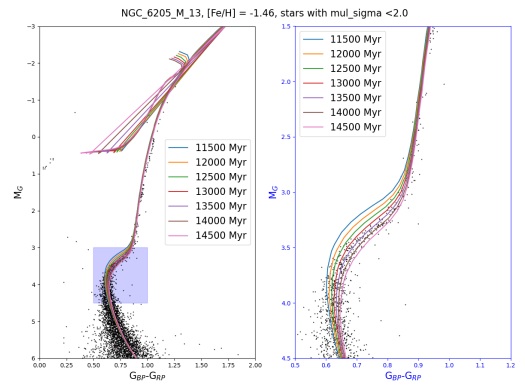
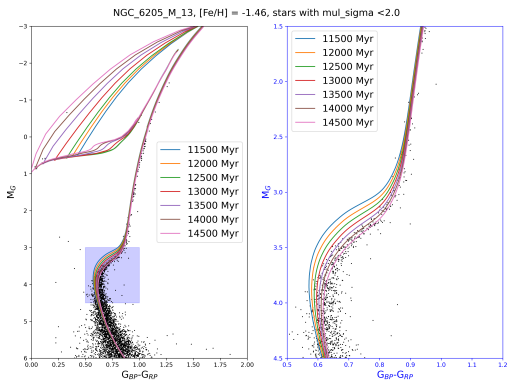
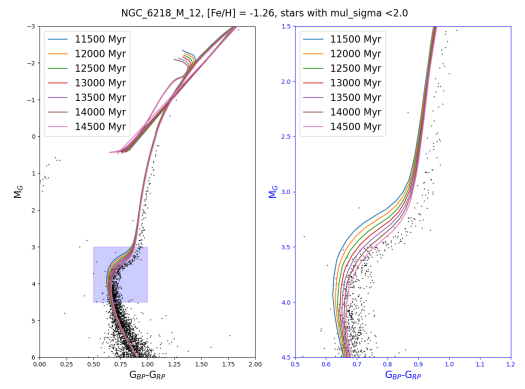
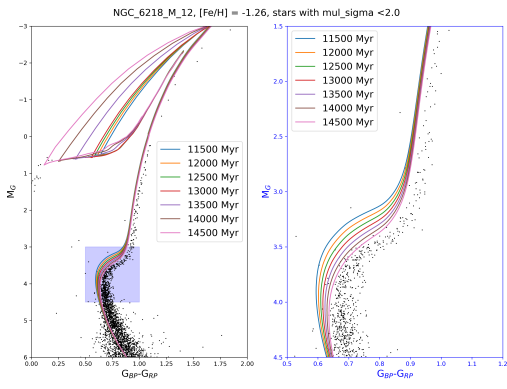


Figure 30: CMDs of all clusters in absolute magnitude with filters applied. Stars with MP less than 0.9 are shown in gray, those eliminated by the crowding ellipse are shown in red, and the stars that pass all the filters and are used for analysis are shown in black. Additionally, a histogram of the membership probabilities is included.

A.3. Comparing between models: BaSTI and PARSEC





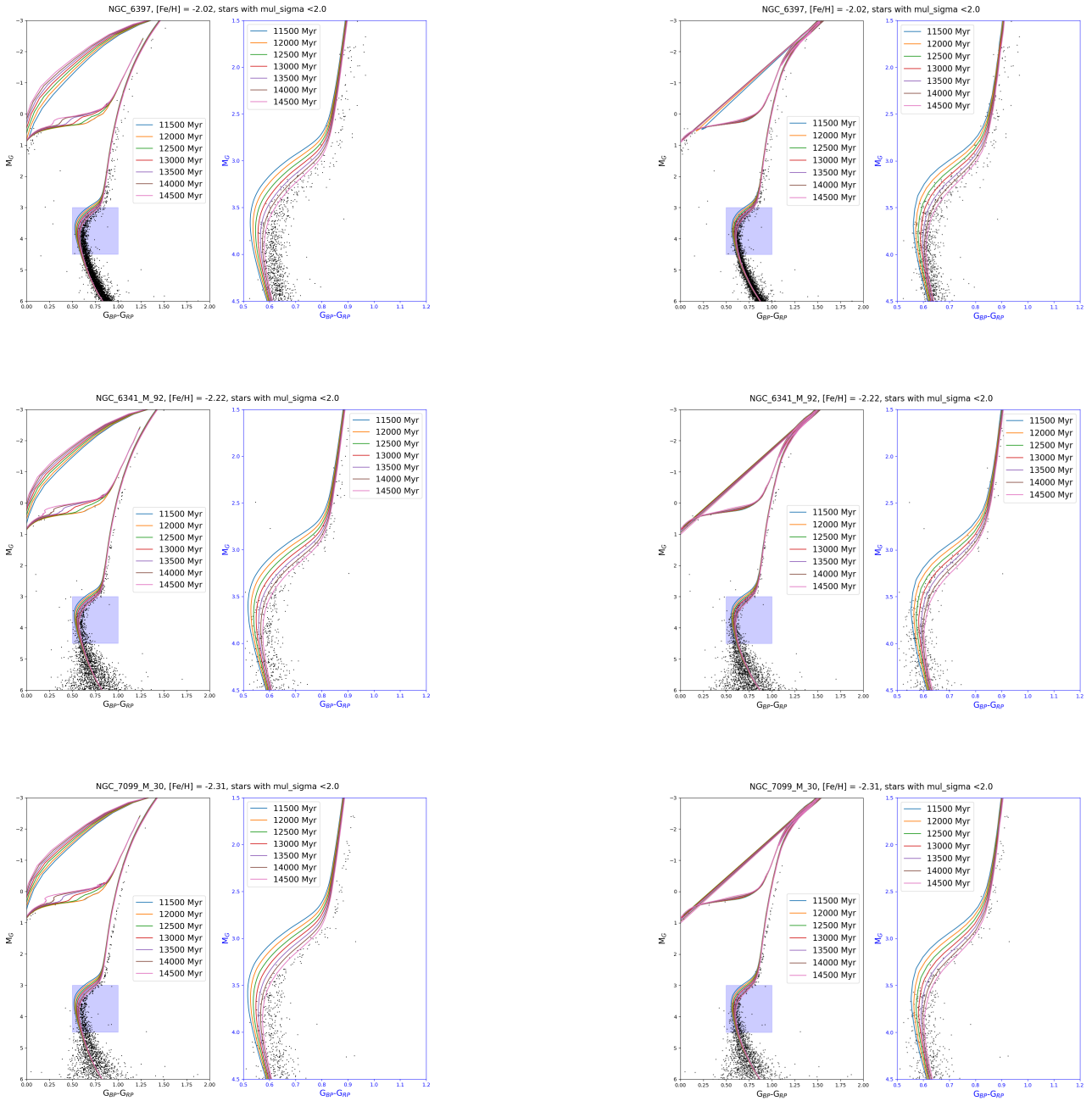
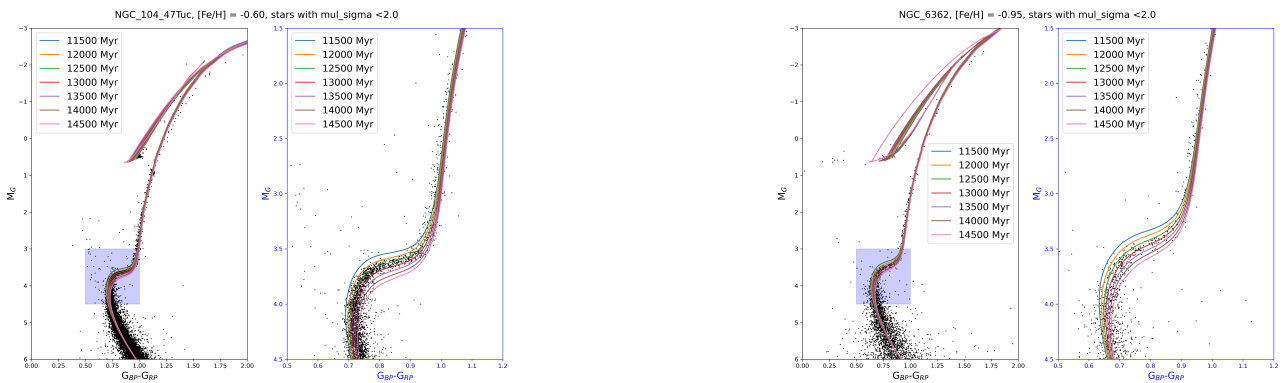


Figure 31: CMD of star selection from each cluster, extinction corrected, superimposed with the BaSTI (left) and PARSEC (right) isochrones.

A.4. Individually BaSTI fits



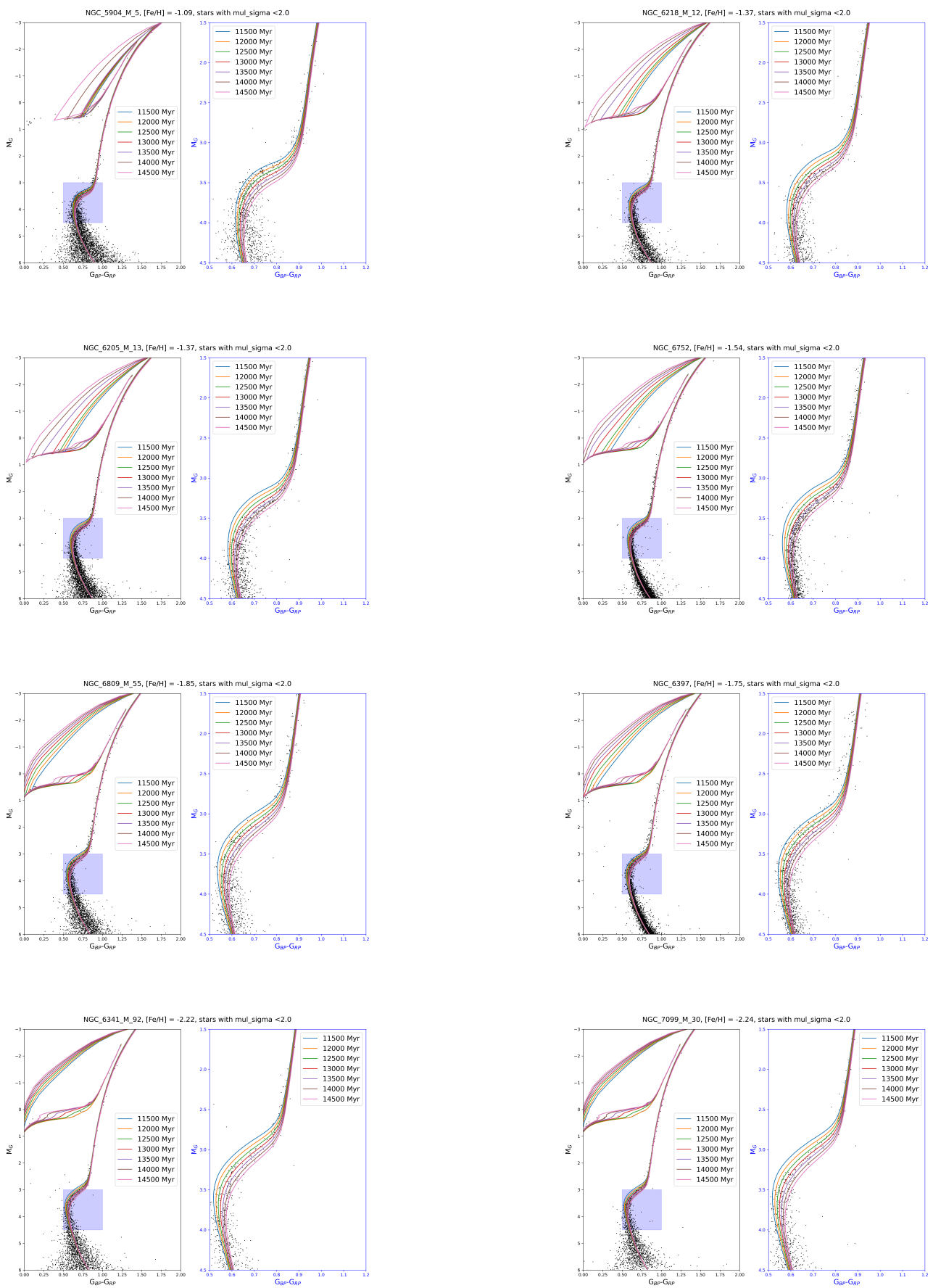


Figure 32: CMD of star selection from each cluster, extinction corrected, superimposed with the manual fitted BaSTI isochrones.

B. Appendix: Synthetic data

B.1. Synthetic data selection at old ages

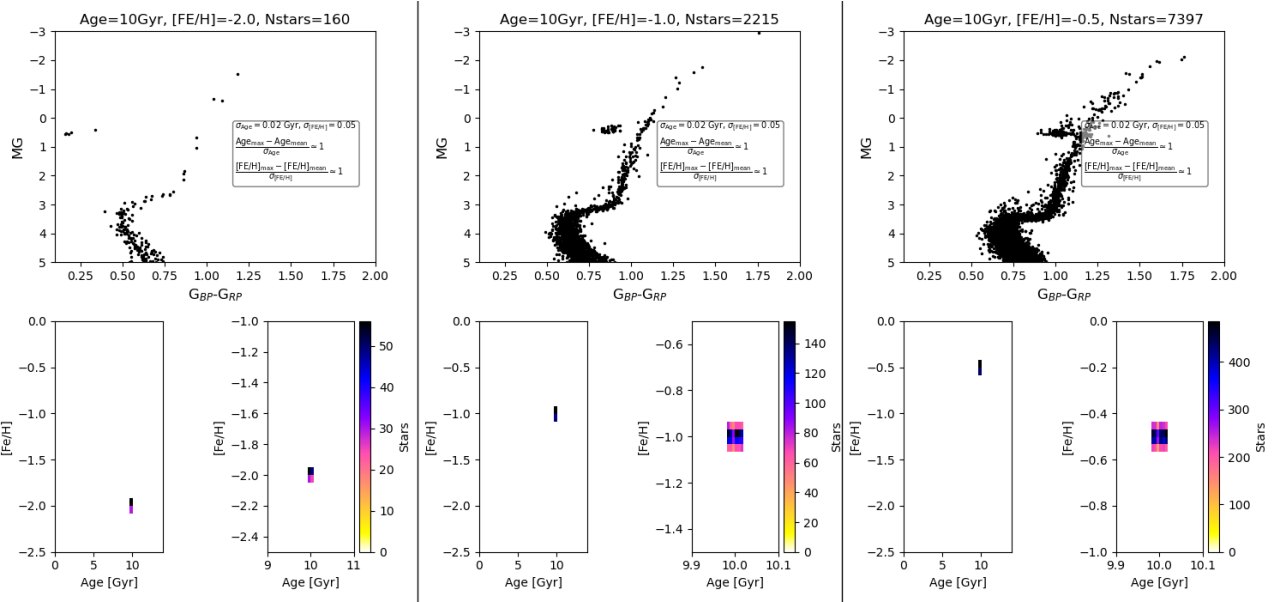


Figure 33: CMD of 3 synthetic globular cluster of 10 Gyr selected by rectangle selection. Also it is included an 2D histogram in age-metallicity plane of selected stars. The cut rectangle is only use for rescaled space in the Gaussian selection.

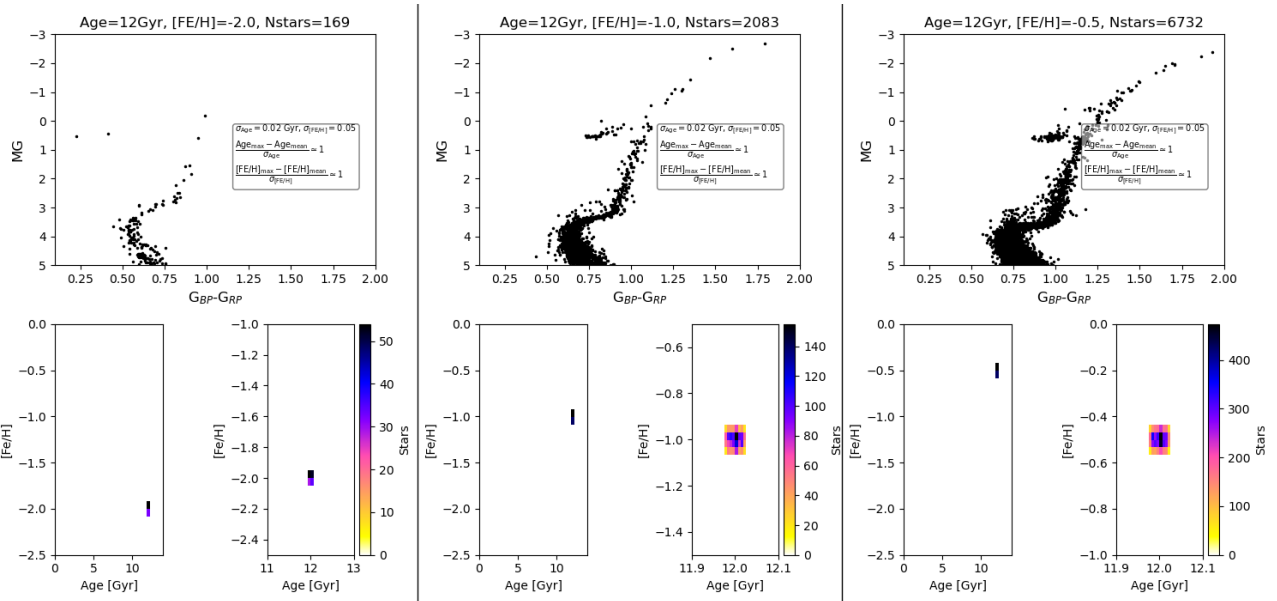


Figure 34: CMD of 3 synthetic globular cluster of 12 Gyr selected by rectangle selection. Also it is included an 2D histogram in age-metallicity plane of selected stars. The cut rectangle is only use for rescaled space in the Gaussian selection.

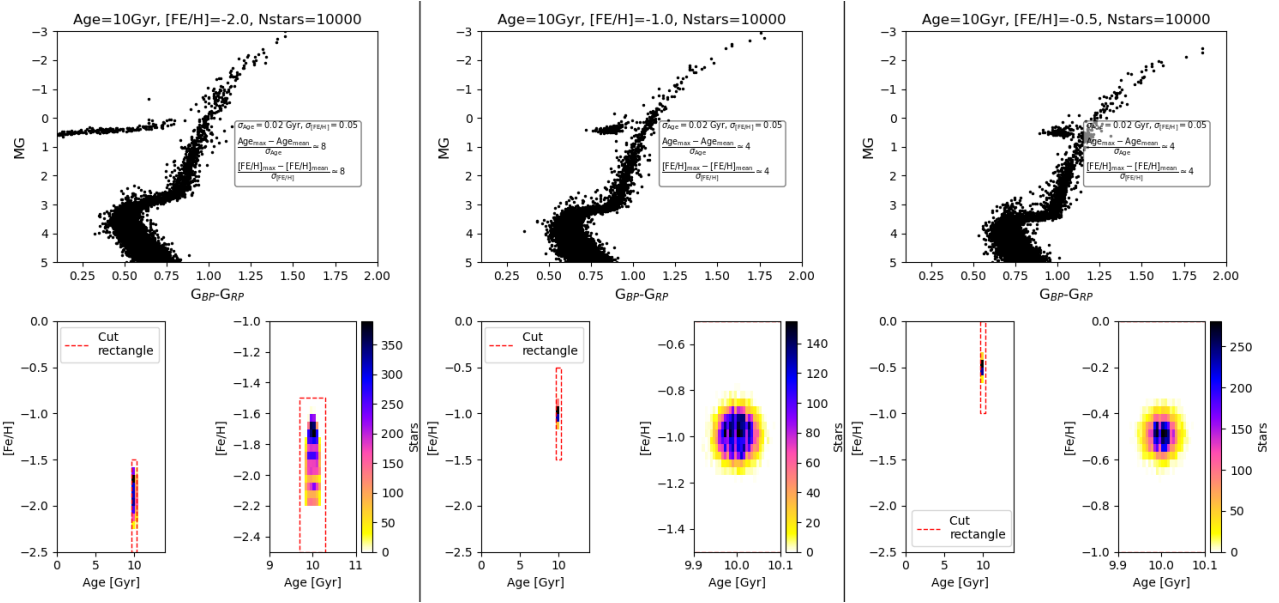


Figure 35: CMD of 3 synthetic globular cluster of 10 Gyr selected by Gaussian selection. Also it is included an 2D histogram in age-metallicity plane of selected stars. The cut rectangle is used for rescaled space.

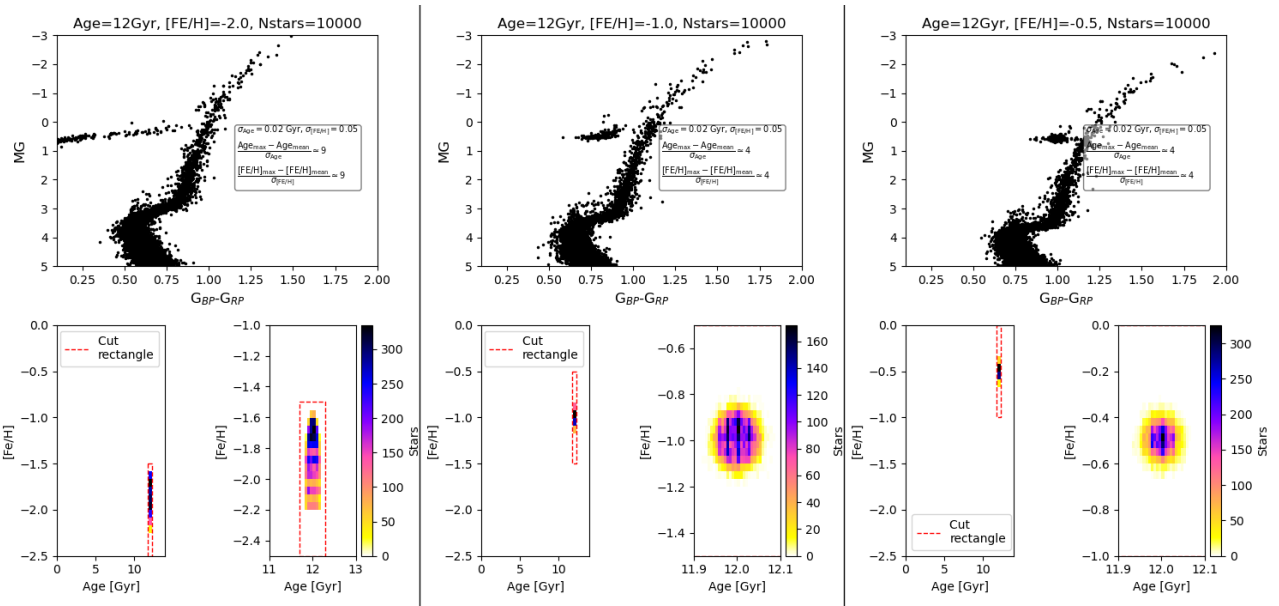


Figure 36: CMD of 3 synthetic globular cluster of 12 Gyr selected by Gaussian selection. Also it is included an 2D histogram in age-metallicity plane of selected stars. The cut rectangle is used for rescaled space.

B.2. Gaussian fitting for the SFH calculation of the 15000 stars sample

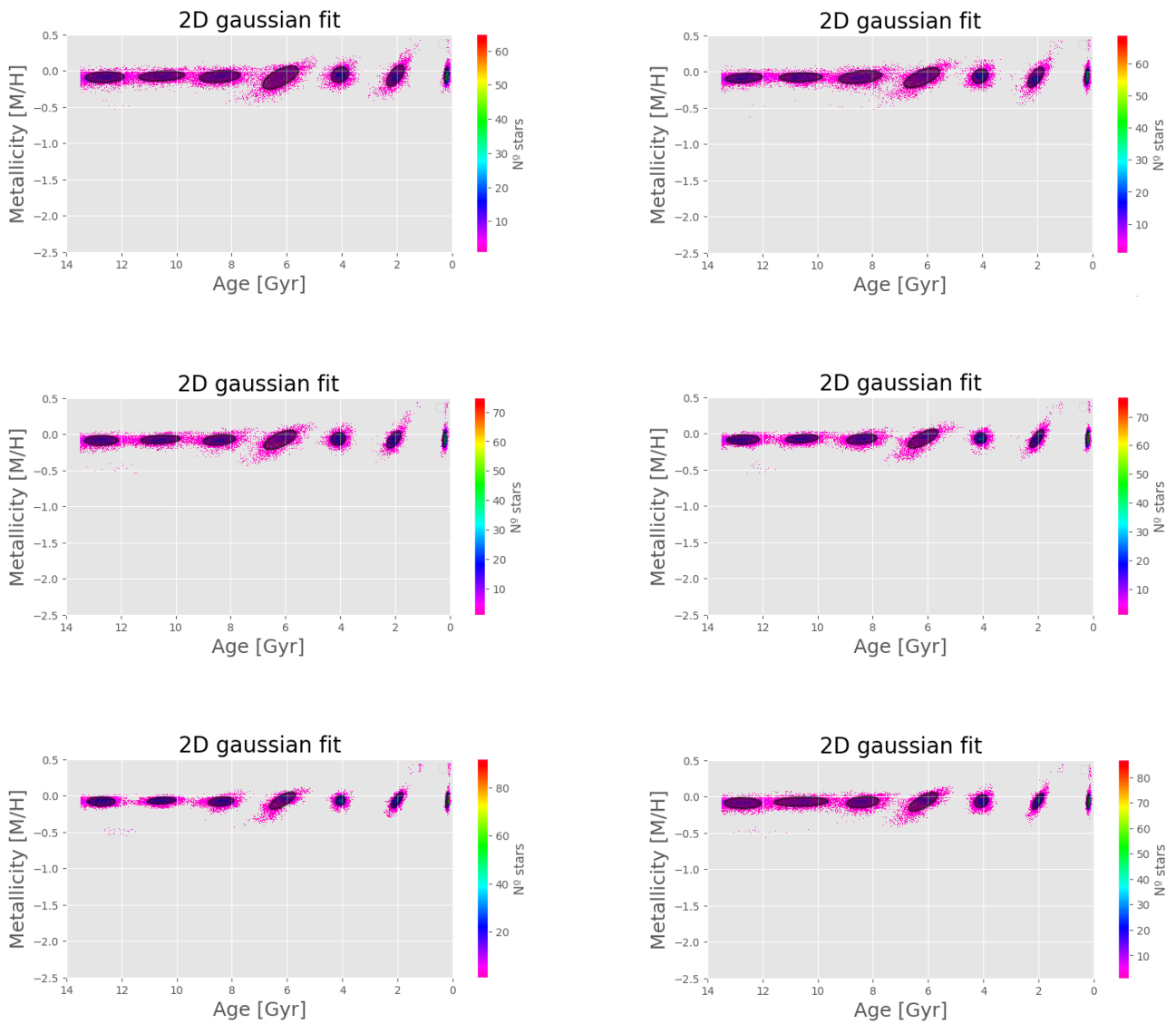


Figure 37: Solution diagram in the age-metallicity plane with the Gaussian fitted for each burst. From left to right different size of age bins is shown, recast 0.5 to recast 1.5. The last figure correspond to the lineal bin size.

B.3. Gaussian fitting for the SFH calculation of the 100000 stars sample

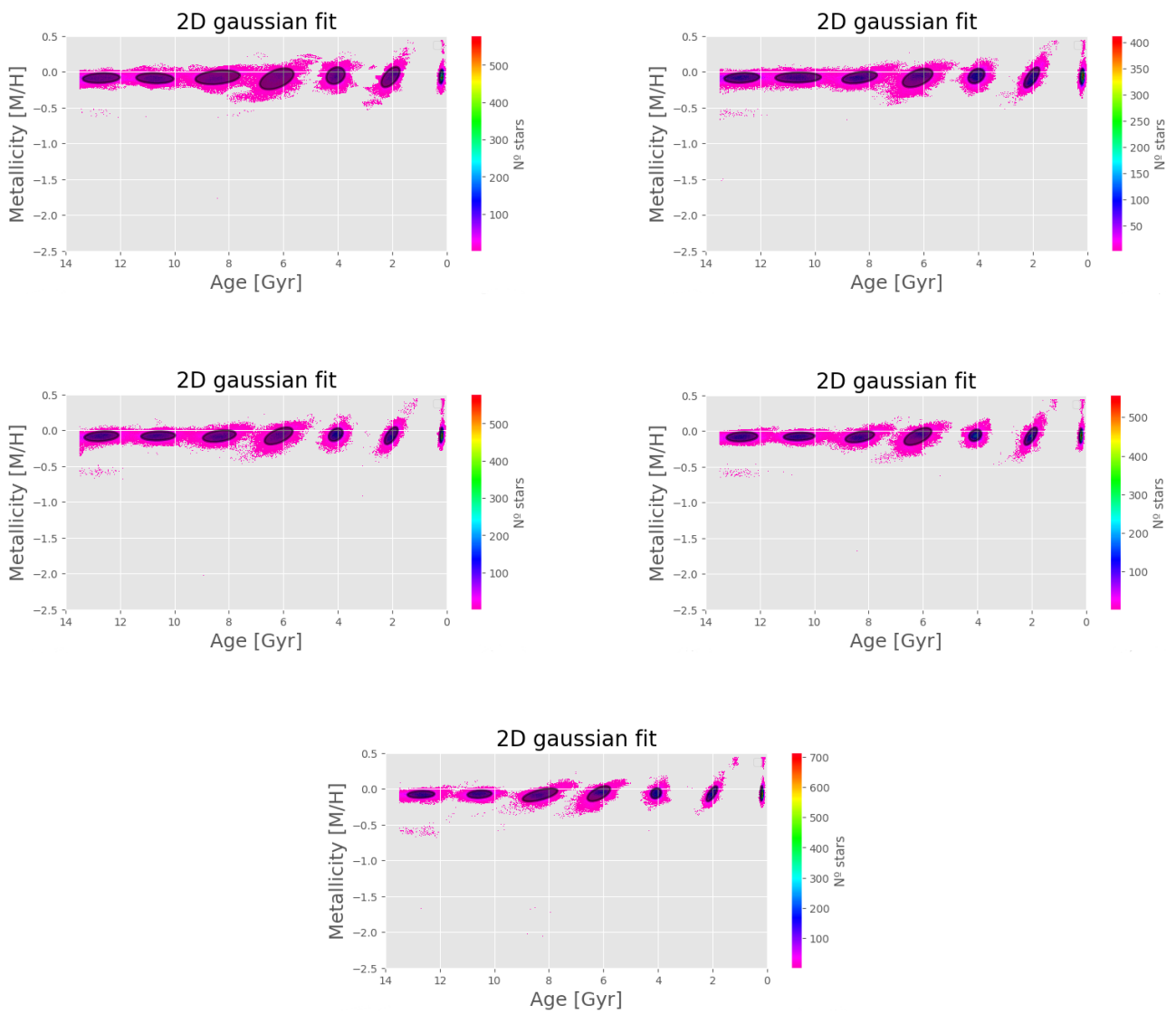


Figure 38: Solution diagram in the age-metallicity plane with the Gaussian fitted for each burst. From left to right different size of age bins is shown, recast 0.5 to recast 1.5. The last figure correspond to the lineal bin size.

B.4. SFH of all recast

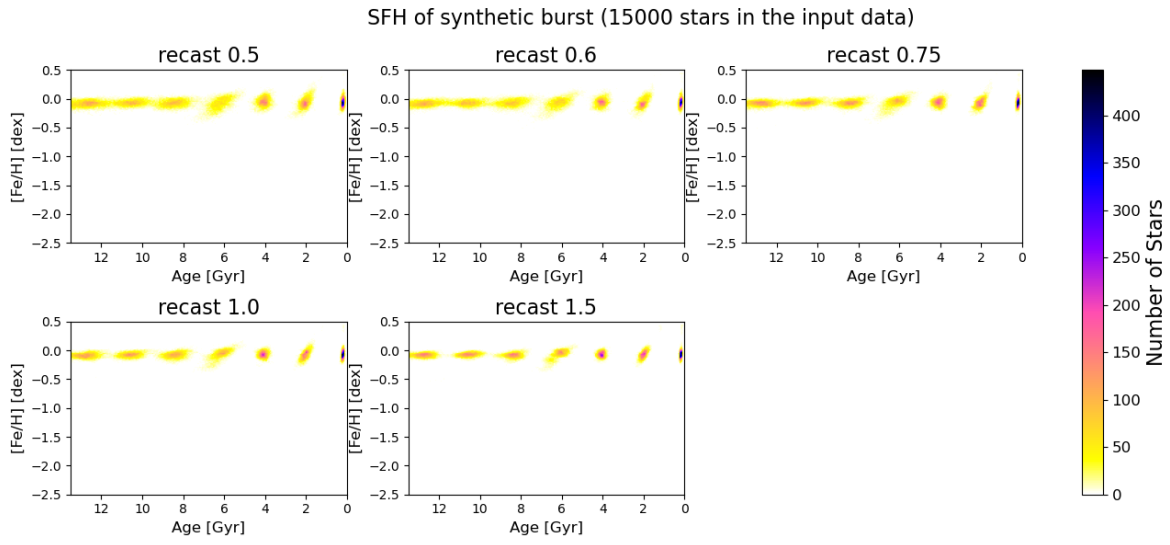


Figure 39: SFH in the age-metallicity plane of synthetic clusters of 15000 stars for all different age bins.

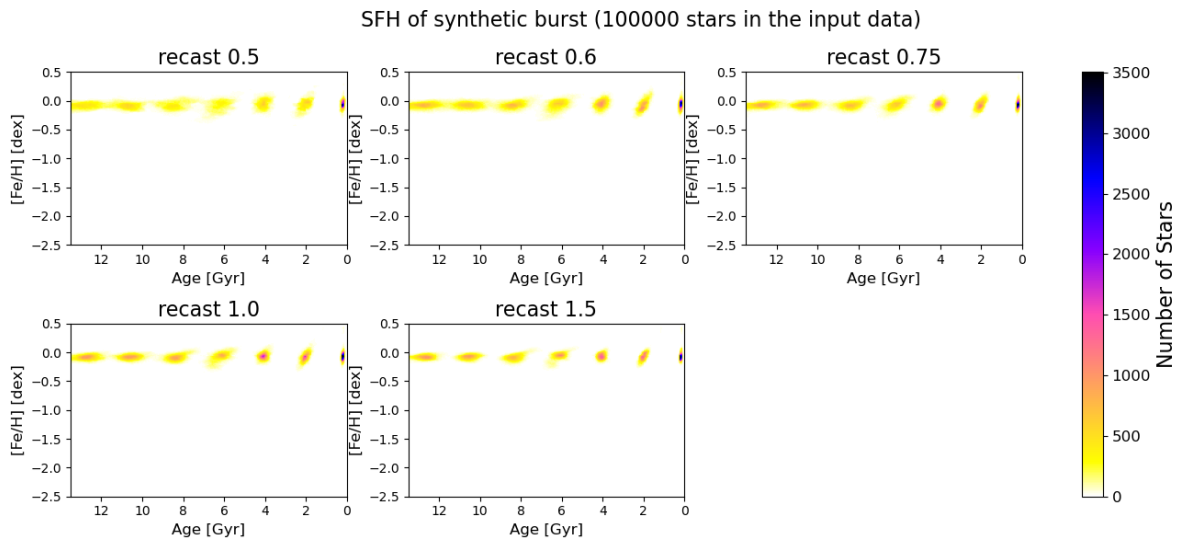


Figure 40: SFH in the age-metallicity plane of synthetic clusters of 100000 stars for all different age bins.

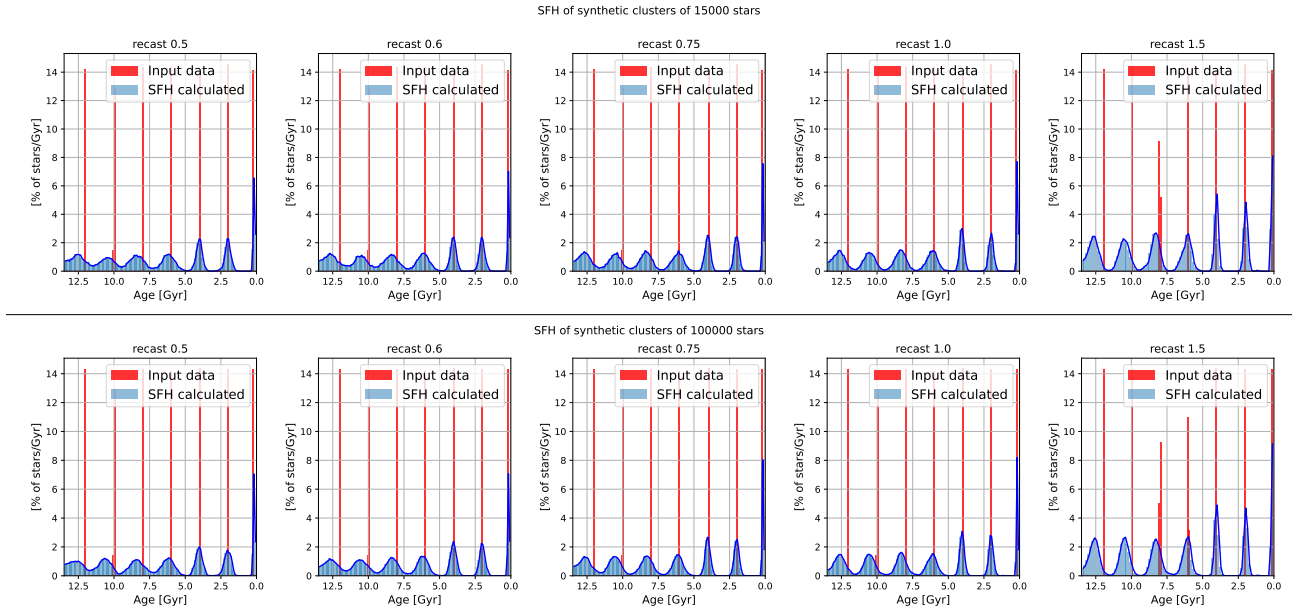


Figure 41: Percentage of stars by age for all age bins size of the synthetic clusters compared with the age histogram of the input stars.

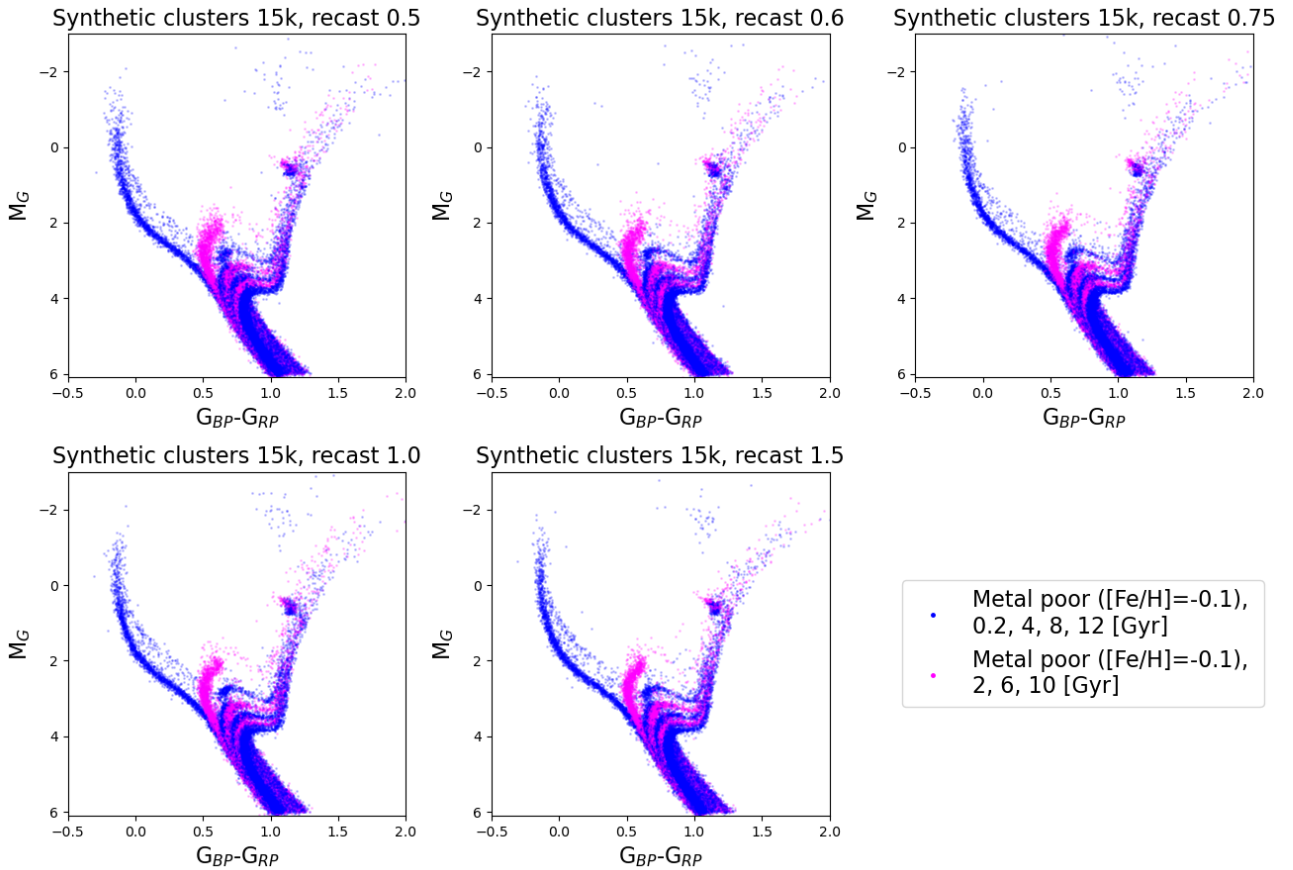


Figure 42: CMDs calculated of all different age bins size for the sample of 15000 in the input CMD.

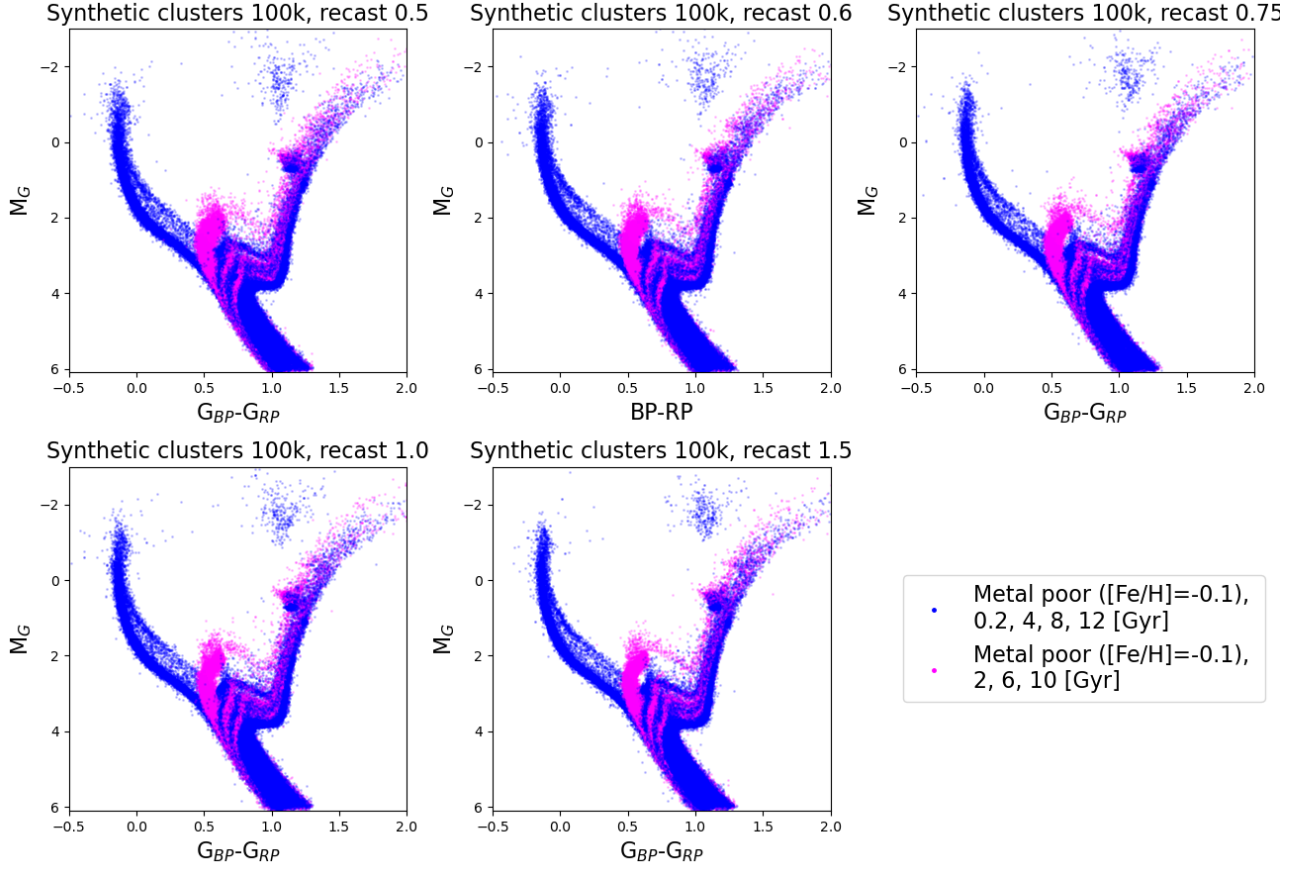


Figure 43: CMDs calculated of all different age bins size for the sample of 100000 in the input CMD.

B.5. Accuracy in age of each age bin size for bursts calculated

BURSTS 15000 stars															
	Burst 0.2 Gyr [Gyr]	Error 0.2 Gyr [Gyr]	Burst 2 Gyr [Gyr]	Error 2 Gyr [Gyr]	Burst 4 Gyr [Gyr]	Error 4 Gyr [Gyr]	Burst 6 Gyr [Gyr]	Error 6 Gyr [Gyr]	Burst 8 Gyr [Gyr]	Error 8 Gyr [Gyr]	Burst 10 Gyr [Gyr]	Error 10 Gyr [Gyr]	Burst 12 Gyr [Gyr]	Error 12 Gyr [Gyr]	Average error [Gyr]
recast 0.5	0.206	0.006	2.050	0.050	4.067	0.067	6.225	0.225	8.430	0.430	10.544	0.544	12.608	0.608	0.130
recast 0.6	0.206	0.006	2.060	0.060	4.082	0.082	6.199	0.199	8.440	0.440	10.604	0.604	12.673	0.673	0.139
recast 0.75	0.205	0.005	2.049	0.049	4.081	0.081	6.198	0.198	8.410	0.410	10.568	0.568	12.713	0.713	0.132
recast 1.0	0.205	0.005	2.034	0.034	4.086	0.086	6.175	0.175	8.395	0.395	10.562	0.562	12.708	0.708	0.122
recast 1.5	0.202	0.002	2.024	0.024	4.082	0.082	6.170	0.170	8.394	0.394	10.550	0.550	12.738	0.738	0.101
Average [Gyr]	0.205	0.004	2.043	0.041	4.080	0.080	6.183	0.192	8.414	0.413	10.566	0.565	12.688	0.686	
BURSTS 10000 stars															
	Burst 0.2 Gyr [Gyr]	Error 0.2 Gyr [Gyr]	Burst 2 Gyr [Gyr]	Error 2 Gyr [Gyr]	Burst 4 Gyr [Gyr]	Error 4 Gyr [Gyr]	Burst 6 Gyr [Gyr]	Error 6 Gyr [Gyr]	Burst 8 Gyr [Gyr]	Error 8 Gyr [Gyr]	Burst 10 Gyr [Gyr]	Error 10 Gyr [Gyr]	Burst 12 Gyr [Gyr]	Error 12 Gyr [Gyr]	Average error [Gyr]
recast 0.5	0.209	0.009	2.063	0.063	4.081	0.081	6.241	0.241	8.413	0.413	10.720	0.720	12.689	0.689	0.157
recast 0.6	0.206	0.006	2.044	0.044	4.073	0.073	6.227	0.227	8.354	0.354	10.609	0.609	12.675	0.675	0.132
recast 0.75	0.206	0.006	2.042	0.042	4.076	0.076	6.172	0.172	8.350	0.350	10.597	0.597	12.679	0.679	0.126
recast 1.0	0.206	0.006	2.038	0.038	4.078	0.078	6.189	0.189	8.324	0.324	10.555	0.555	12.657	0.657	0.122
recast 1.5	0.205	0.005	2.025	0.025	4.076	0.076	6.167	0.167	8.322	0.322	10.540	0.540	12.686	0.686	0.110
Average [Gyr]	0.207	0.007	2.042	0.041	4.077	0.077	6.199	0.197	8.353	0.351	10.604	0.601	12.677	0.677	

Table 6: Center in age of each calculated burst. For this purpose, a Gaussian is fitted to each burst and the center of this Gaussian corresponds to the assumed age for each calculated burst. Also the error in the predicted age is calculated, this is the difference between the real age of the burst in the input data and the center of the Gaussian. It is shown for the test performed with the 2 input samples and for each age bin size.